

CEBAF Program Advisory Committee Six (PAC6) Proposal Cover Sheet

This proposal must be received by close of business on April 5, 1993 at:

CEBAF
User Liaison Office
12000 Jefferson Avenue
Newport News, VA 23606

Proposal Title

Longitudinal/Transverse Cross Section Separation in $p(e, e'K^+) \Lambda(\Sigma^0)$ for $0.5 \leq Q^2 \leq 2.0$ (GeV/c)², $W \geq 1.7$ GeV, and $t_{\min} \geq 0.1$ (GeV/c)².

Contact Person

Name: O. Keith Baker

Institution: Hampton University

Address: Department of Physics, Hampton University

Address:

City, State ZIP/Country: Hampton, VA 23668 USA

Phone: (804) 727-5820 or 249-7343

FAX: (804) 727-5188 or 249-7363

E-Mail → BITnet: BAKER@CEBAF

Internet:

If this proposal is based on a previously submitted proposal or letter-of-intent, give the number, title and date:

CEBAF Proposal PR-91-022 Measurement of the Kaon Form Factor
for $0.5 \leq Q^2 \leq 2.0$ (GeV/c)²

Fall 1991

CEBAF Use Only

Receipt Date: 4/5/93

Log Number Assigned: PR 93-018

By: J

PROPOSAL UPDATE PR91-022

Longitudinal/Transverse Cross Section Separation in $p(e, e'K^+)\Lambda$ (Σ)
for $0.5 \text{ GeV}^2/c^2 \leq Q^2 \leq 2.0 \text{ GeV}^2/c^2$, $W \geq 1.7 \text{ GeV}$, and $t_{\min} \geq 0.1 \text{ GeV}^2/c^2$

O.K. Baker⁺(Spokesman), K. Beard, S. Beedoe, W. W. Buck⁺, K. M. Maung, L. Tang⁺

Physics Department, Hampton University

+ and jointly, Physics Division, CEBAF

D. Abbott^o, L. Cardman, R. Carlini, Y. Chen, D. Mack,

S. Majewski, J. Mitchell, W. Vulcan, S. Wood

Physics Division, CEBAF

o and Physics Department, College of William and Mary

B. Zeidman

Physics Division, Argonne National Laboratory

E. Hungerford, K. Lan, B. Mayes

Physics Department, University of Houston

J. Napolitano

Department of Physics, Rensselaer Polytechnic Institute

S. Mtingwa

Physics Department, North Carolina A & T State University

C.C. Chang, P. Markowitz

Department of Physics and Astronomy, University of Maryland

R. Madey

Department of Physics, Kent State University, and

Department of Physics, Hampton University

T. Angelescu, A. Mihul

Bucharest University, Bucharest, Romania

CEBAF EXPERIMENT MAJOR REQUIREMENTS

Beam Time (Days)	14.5
Beam Energies (GeV)	2.4, 3.2, 3.5, 4.0
Beam Type	Unpolarized
Beam Current	$\leq 50 \mu\text{A}$
Targets Needed	Liquid H ₂
Power Deposition	≤ 50 watts

BEAM TIME REQUEST

	Time (Days)
Data Acquisition	9.5
Setup and Checkout	1.0
Angle Changes	0.2
Background Studies	2.0
Contingency (15%)	1.8
TOTAL BEAM TIME	14.5

SPECTROMETER REQUIREMENTS

	Electron Arm	Hadron Arm
Solid Angle	5 msr	4 msr
Momentum Acceptance	20%	40%
Momentum Resolution	$\leq 10^{-3}$	$\leq 10^{-3}$
Min Scatt Angle	14.5	13.4
Max Scatt Angle	61.4	23.6
Min Central Momentum	0.7 GeV	1.0 GeV
Max Central Momentum	2.4 GeV	1.7 GeV
Particle i.d. Required	π^-/e^-	$\pi^+/K^+, p/K^+$
Required Ratio	0.01	0.005

ABSTRACT

This experiment will provide a fundamental measurement of the kaon electroproduction cross section in the reaction $p(e, e'K^+)\Lambda(\Sigma)$ in a way never before accomplished. Future experiments exploring this reaction on heavier nuclei and in various kinematic ranges will need the results of this proposed experiment. It is proposed to detect the scattered electron and the electroproduced kaon in coincidence using the Hall C spectrometers. The cross section for kaon electroproduction in this experiment has four terms. These four terms are due to (i) unpolarized transverse, (ii) longitudinal, (iii) interference between transverse, and (iv) interference between longitudinal and transverse, virtual photons. This experiment aims to separate the four terms individually, and in particular, provide the first measurements of the longitudinal and transverse cross sections for $0.50 \leq Q^2 \leq 2.00 \text{ GeV}^2/c^2$. Once this separation has been achieved, there are several physics issues which can be studied in ways not feasible before now. The dependence of the transverse cross section on Bjorken x will be determined for $0.1 \leq x \leq 0.4$. There is the potential for an estimate of the strangeness content of the proton from this measurement. The t -dependence of the longitudinal cross section will be determined for $0.1 \leq t \leq 0.5 \text{ GeV}^2/c^2$ at $Q^2 = 0.5 \text{ GeV}^2/c^2$ and $1.0 \text{ GeV}^2/c^2$. Then, employing the Chew-Low extrapolation technique, the Kaon Electromagnetic Form Factor can, in principle, be determined for these two Q^2 points. Additionally, this experiment will separate the two interference cross sections at $Q^2 = 0.5 \text{ GeV}^2/c^2$ and $1.0 \text{ GeV}^2/c^2$. In each case, the missing mass of the reaction will be determined (thus identifying both Λ and Σ hyperons). There is then a possible QCD signature in the measurement of the cross section versus Q^2 comparing Λ -particle final states with Σ -particle final states. Despite the importance of this measurement, no previous data exists for the separated contributions as this proposed experiment aim to achieve.

1. OVERVIEW

1.1 Introduction

Electron scattering has proven to be an ideal tool for investigating nucleon and nuclear structure¹⁻⁶. The electromagnetic interaction, the predominant interaction in electron scattering, is known and minimally disturbs the target, compared to other interactions such as those using hadronic probes. The electron scattering variables, initial and final energy and scattering angle, can be varied in such ways as to vary the energy transfer and momentum transfer to the target. This brings out new and interesting features of nucleon and nuclear structure not directly attainable otherwise and allows measurement of the Fourier transform of the transition charge and current densities^{1,3}. Then their detailed microscopic spatial structure can be studied. Additionally, varying the electron kinematics allows the separation of the various combinations of nuclear amplitudes contributing to the transition. The experimental facility planned at the Continuous Electron Beam Facility (CEBAF) is ideally suited for such a study⁷.

This experimental proposal uses electron scattering to study various features of the nucleon systems, and of their mesonic, quark, and gluon substructure⁸⁻¹⁵. The study proposed here uses the reaction



on the proton. (The energies proposed here will be high enough so that Σ hyperons are produced in addition to Λ s.)

The program will be carried out by detecting, in coincidence, the scattered electron and the electroproduced kaon. The high duty factor of the CEBAF machine should allow the implementation of coincidence experiments and measurement of final strange systems in coincidence with the scattered electrons in a systematic way where, because of the low duty factors of existing high energy electron machines, only exploratory coincidence measurements were achievable previously.

1.2 Theoretical Background and Kinematics

The general form of the electron scattering cross section for detection of one nucleon or meson in coincidence with the final scattered electron in the Born approximation has been known for some time. For this experiment none of the spins, initial or final, are observed. The cross section can be written as a linear combination of four terms which completely characterize the dependence of the cross section on the nucleon or nucleus.

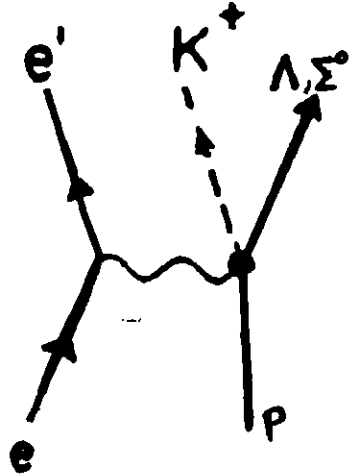


Figure 1. The Feynman diagram representation of the electroproduction of kaons. The electron scatters, emitting a virtual photon which scatters off of the proton yielding a K^+ meson (kaon) and a Λ or Σ .

The process considered is shown in Fig. 1. The process may be written as

$$e^- + A \rightarrow e^- + B + C \quad (3)$$

which may be related to the associated photonuclear reaction^{1,3}

$$\gamma_v + A \rightarrow B + C \quad (4)$$

in a calculation to first order in the electromagnetic coupling constant

$$\alpha = \frac{e^2}{4\pi} \approx \frac{1}{137}. \quad (5)$$

This association is justified because the corrections to the result are expected to be, at most, of order α^2 , several orders of magnitude lower and therefore insignificant for the purposes of this analysis¹⁻⁶.

The kinematic variables of the $(e, e'K^+)$ cross section (and $(e, e'X)$ in general) are shown in Fig. 2. The incident (scattered) electron with momenta k (k') lies in the same plane - the electron scattering plane - as the virtual photon. The recoiling K^+ (or ejectile, X , in general) of momenta p' and the residual system of momenta p_R lie in a different plane - the ejectile plane. Note that the virtual photon lies in both planes. The angle between the electron scattering plane and the ejectile plane is ϕ , the out-of-plane angle. The polar angle between the virtual photon and the ejectile is $\theta_{\gamma, X}$ while the polar angle between the incident and scattered electron is θ_e .

The form of the kinematic variables is well known for the reaction

$$e + p \rightarrow e' + K^+ + \Lambda(\Sigma^0) \quad (6)$$

or in terms of the particles' four-momenta

$$k_1 + p_1 = k_2 + K + p_2 \quad (7)$$

where the notation used is¹⁷

$$l = (k_0, l) \quad (8)$$

Here k_1 and k_2 refer to the initial and final electron (of mass μ), p_1 and p_2 to the initial and final nucleon (of mass m_N), and K refers to the produced meson (of mass m_K). $K^2 = m_K^2$ is the mass squared of the kaon in this case, and similarly $p^2 = m_N^2$ for the nucleon. The four momentum transferred from the electron to the proton is q , the virtual photon four-momentum.

$$q = k_1 - k_2 \quad (9)$$

and

$$q^2 = -Q^2 = -4k_{o1}k_{o2}\sin^2(\theta_e/2) \quad (10)$$

where $k_{o1} = E_e$ ($k_{o2} = E'_e$) is the initial (final) electron energy and θ_e is the electron scattering angle, neglecting the electron mass for the energies and momenta considered here.

The kinematic variable t is then defined as

$$-t = (q - K)^2 = q^2 + m_K^2 - 2q \cdot K = 2m_N^2 - 2p_1 \cdot p_2 \quad (11)$$

or as it is sometimes written

$$t = t_{\min} - 4|q||K|\sin^2(\theta_{\gamma, K}/2) \quad (12)$$

with

$$t_{\min} = (q_0 - K_0)^2 - (|\mathbf{q}| - |\mathbf{K}|)^2 \quad (13)$$

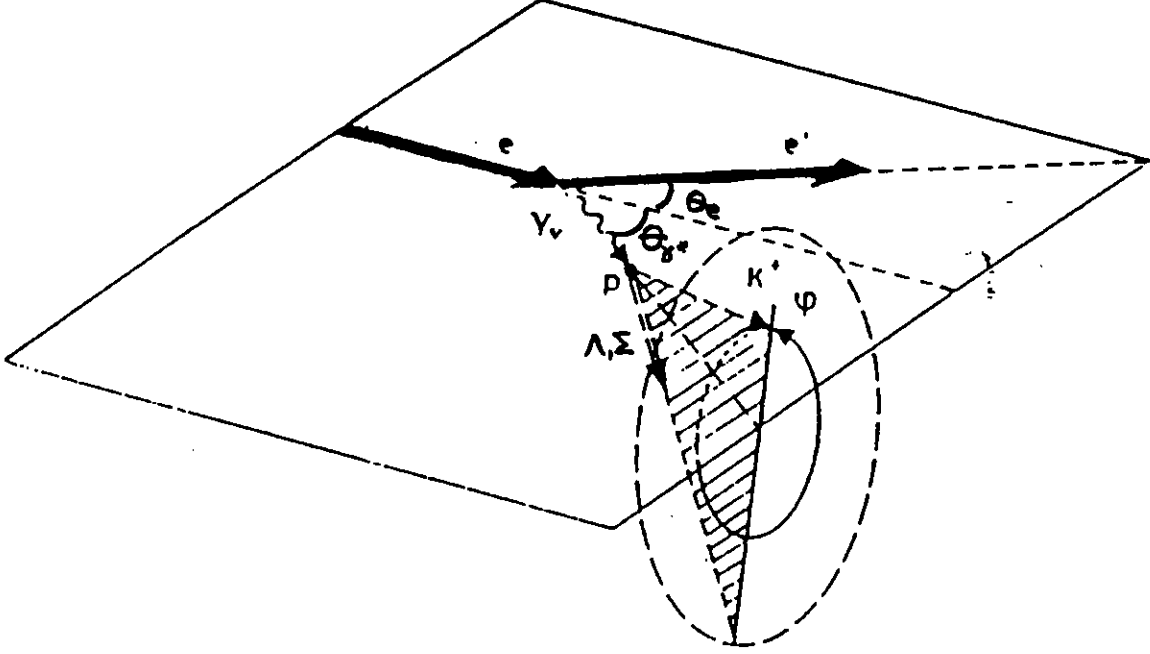


Figure 2. The kinematic variables used in the kaon electroproduction process.

It has been shown¹⁻⁵ that the general form of the cross section for the reaction listed above for an unpolarized beam and target and no detected polarization in the final state can be written as

$$\frac{d^3\sigma}{d\Omega_e dE' d\Omega_X} = \frac{\sigma_M r}{4\pi M_T} \{V_L R_L + V_T R_T + V_{TT} R_{TT} \cos 2\phi_X + V_{LT} R_{LT} \cos 2\phi_X\} \quad (14)$$

where σ_M is the Mott cross section, M_T is the target proton mass, and r , the recoil factor, is

$$r = \frac{W}{M_T} \frac{1}{\left(1 + \frac{\nu'_p - E_{p'} q \cos \theta_e}{M_{Tp'}}\right)} \quad (15)$$

The kinematic factors are

$$\begin{aligned}
V_L &= \frac{Q^2}{q^2} & V_T &= \frac{Q^2}{2q^2} + \tan^2 \frac{\theta_e}{2} \\
V_{TT} &= \frac{Q^2}{2q^2} & V_{LT} &= -\frac{Q}{\sqrt{2}|q|} \left(\frac{Q^2}{2q^2} + \tan^2 \frac{\theta_e}{2} \right)^{1/2}
\end{aligned} \tag{16}$$

where $Q^2 = q^2 - \nu^2$. The response functions, R_i are defined in reference [1].

The cross section can be written in the more useful form for our purpose

$$\frac{d^3\sigma}{d\Omega_e dE'_e d\Omega_{K^+}} = \Gamma \frac{d\sigma}{d\Omega_{K^+}} = \Gamma (\sigma_U + \epsilon\sigma_L + \epsilon\cos 2\phi\sigma_{TT} + \sqrt{\frac{\epsilon(\epsilon+1)}{2}} \cos\phi\sigma_{LT}) \tag{17}$$

The cross section formula using invariant variables can be written in the more familiar form

$$\frac{1}{\Gamma_T} \frac{d^4\sigma}{dsdq^2 dt d\phi} \equiv \frac{d\sigma}{dt} |_{K^+} = \sigma_U + \epsilon\sigma_L + \epsilon\cos 2\phi\sigma_{TT} + \sqrt{\frac{\epsilon(\epsilon+1)}{2}} \cos\phi\sigma_{LT} \tag{18}$$

where

$$\Gamma = \frac{\alpha(s - m_N^2)}{4(2\pi)^2 E_e^2 m^2 |Q^2| (1 - \epsilon)} \tag{19}$$

is related to the 'flux' of virtual photons, and

$$\epsilon = 1 + 2 \left| \frac{\mathbf{k}}{Q^2} \right|^2 \tan^2 \theta_e / 2 \tag{20}$$

is the virtual photon polarization parameter.

The first term, σ_U , represents the cross section for photoproduction by a virtual photon, unpolarized, with the photon spin vector in a plane transverse to the photon direction of motion. The term $\epsilon\sigma_L$ includes the cross section arising from longitudinally polarized photons where the virtual photon's spin vector has a component parallel to its direction of motion. ϕ is the azimuthal angle between the electron scattering plane and the virtual photon-kaon plane. When the kaon is produced at an out-of-plane angle ϕ (with respect to the electron scattering plane), the transverse photons can be polarized parallel or perpendicular to the $K^+\Lambda/\Sigma$ production plane. The term $\epsilon\sigma_{TT}\cos 2\phi$ contains the cross section arising from the interference between the transverse components of this virtual photon polarization. The last term in equation (17), $[\frac{\epsilon(\epsilon+1)}{2}]^{1/2}\sigma_{LT}\cos\phi$ is proportional to the cross section arising from the interference between the transverse and longitudinal photon polarizations. All the cross sections in equations (17) and (18) are functions of Q^2 , W , and θ_{K^+} (or, in this case, t), where $Q^2 = -q^2$ is the 4-momentum squared carried

by the virtual photon, W is the total energy of the system in the center of mass of the reaction products, θ_{K^+} is defined in Fig. 2, and t is the square of the difference between the virtual photon 4-momentum and the kaon 4-momentum. The quantities θ_{K^+} and t yield essentially the same information in this study. A more convenient expression for ϵ , the virtual photon polarization parameter, written in terms of the variables given in Table I is:

$$\epsilon^{-1} = 1 + 2\left(1 + \frac{\nu^2}{Q^2}\right)\tan^2(\theta_e/2). \quad (21)$$

where ν is the virtual photon energy and θ_e is the electron scattering angle with respect to the incident beam direction.

2. PHYSICS MOTIVATION

2.1 The Ratio Σ^0 and Λ Production and the Strangeness Content of the Protons

In the parton description of baryons, a nucleon or meson is composed of (constituent) quarks surrounded by quark-antiquark ($q\bar{q}$) pairs and gluons in a quark-gluon 'sea'. A K^+ -meson is then an $u\bar{s}$ quark pair surrounded, presumably, by $u\bar{u}$, $d\bar{d}$, and $s\bar{s}$ sea quarks and gluons. A proton is a uud triplet of constituent quarks surrounded by the sea quarks and gluons. In the electron scattering reaction, a virtual photon carries the transferred momentum from the electron to a quark (or gluon or $q\bar{q}$ pair) in the proton. The fraction of the momentum carried by the struck quark is measured by the Bjorken variable $x = Q^2/2m\nu$, a dimensionless variable. Here Q^2 is the four-momentum transfer carried by the photon, m is the kaon mass, and ν is the photon energy. In the arrangement proposed for Hall C, x can be varied in the course of this experiment between $0.1 \leq x \leq 0.4$. This can be performed for separated response functions as detailed earlier.

In some past publications, data on reactions (1) and (2) above were presented for the K^+ produced along the virtual photon direction. The cross sections for these reactions are written as

$$\frac{d\sigma}{d\Omega_{K^+}}(ep \rightarrow eK^+\Lambda) \quad (22)$$

$$\frac{d\sigma}{d\Omega_{K^+}}(ep \rightarrow eK^+\Sigma) \quad (23)$$

respectively. As shown in Fig. 3, previous data reveal that the $(K^+\Sigma)$ cross section decreases faster with increasing Q^2 than the $(K^+\Lambda)$ cross section¹⁸. Two possible explanations have been forwarded to explain this phenomenon.

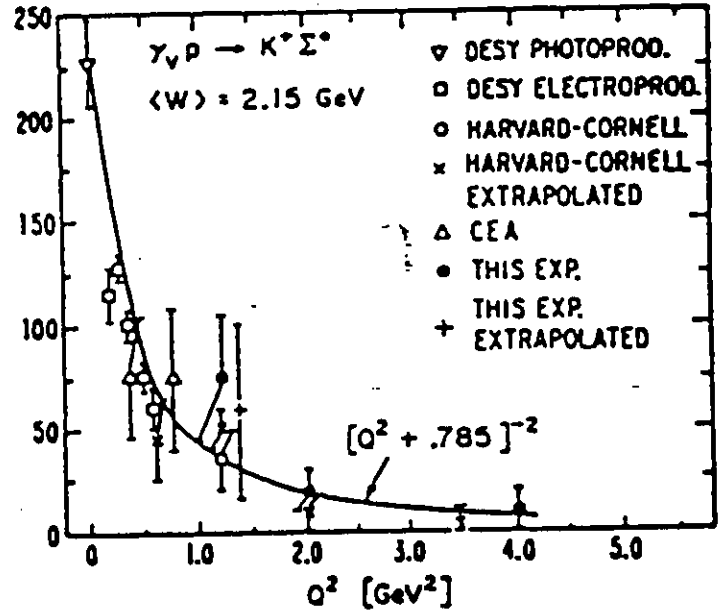
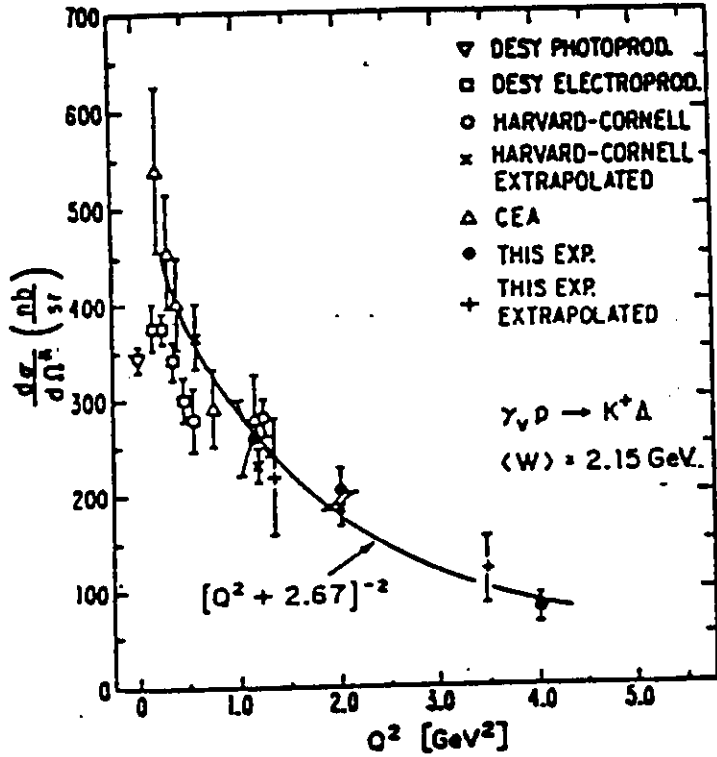


Figure 3. A comparison of the cross section for electroproduction of kaons and Λ particles with that for electroproduction of kaons and Σ particles as shown in reference 18.

Firstly, in a quark-parton model, the steeper Q^2 -dependence of Σ^0 production in comparison with Λ production is interpreted as a consequence of the decrease of the ratio $F_1^{\gamma n}/F_1^{\gamma p}$, the deep inelastic electron-nucleon structure functions of the neutron and proton, as Bjorken x goes to 1^{19} . In the limit $x \rightarrow 1$, the production of kaons in the direction of the virtual photon from u-quarks tends to leave behind an isospin-zero-pair of u-d quarks, that is to say an isospin-zero core. Then the electroproduction of isospin (I)=1 Σ baryons is suppressed compared to $I=0$ Λ baryons.

In Fig. 4 is shown the prediction for the upper and lower limit of the ratio of transverse cross sections. These limits were determined by minimum and maximum estimates of the strange quark contribution from the quark 'sea'; that is, the $s\bar{s}$ pair

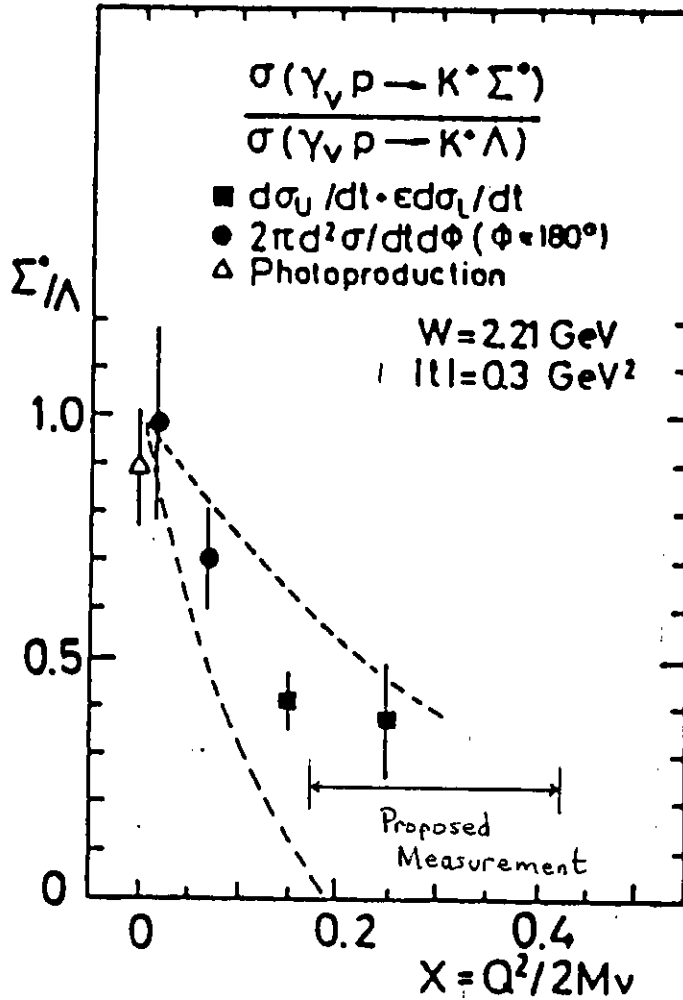


Figure 4. Ratio of cross sections for kaon electroproduction with a Λ or Σ particle in the final state. The curves indicate limits on the strangeness content of the proton from reference 21. Also shown is the region of x accessed in this proposed experiment and the expected accuracy of the measurement.

contribution to the sea. The Nachtmann model should be applied strictly to the transverse cross section σ_U only. Because all experiments to date do not separate the transverse and longitudinal cross sections it can be expected that some of the observed effect might be due to the longitudinal cross section which can be dominated by K-exchange. The present experimental program will separate the transverse and longitudinal cross

sections¹⁹⁻²¹ and allow a more appropriate analysis of the model.

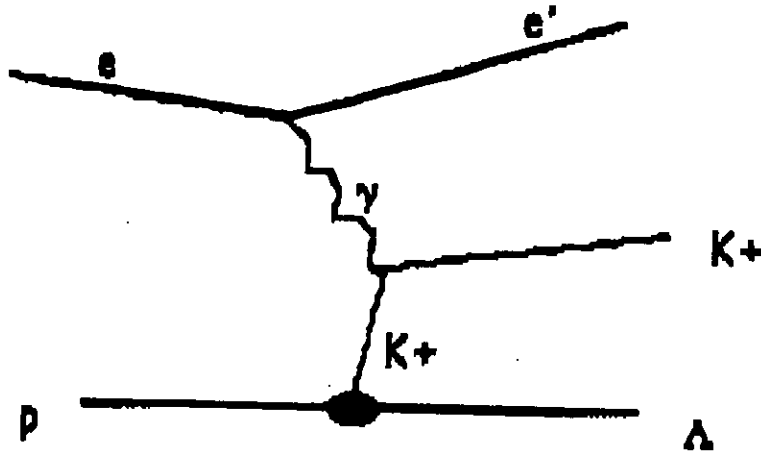


Figure 5. The main contribution to the longitudinal cross section is expected to come from kaon exchange as shown here.

Kaon exchange is the second possible explanation of the Σ^0/Λ ratio cross section¹⁴. The main contribution to σ_L is expected from the exchange of a K^+ -meson as shown in Fig. 5. Then, because the coupling constant $g_{pK\Lambda}^2 \gg g_{pK\Sigma}^2$, the cross section for $K^+\Lambda$ production is favored. Because the contributing terms $\sigma_U + \epsilon\sigma_L$ have not been separated in a single experiment previously^{18,19,22}, there is no experimental evidence for σ_L dominating the $K^+\Lambda$ channel.

2.2 The Kaon Electromagnetic Form Factor

Single kaon electroproduction could be used to determine the kaon form factor²³⁻²⁶ for spacelike values of the photon mass squared ($q^2 < 0$) where

$$q^2 = (k' - k)^2 = (E'_e - E_e)^2 - (|\mathbf{k}'| - |\mathbf{k}|)^2 \quad (24)$$

(This is similar to the work done to extract the pion form factor^{17,27-37}. The analysis of the data to extract the form factor requires use of the Chew-Low extrapolation procedure to be explained below.)

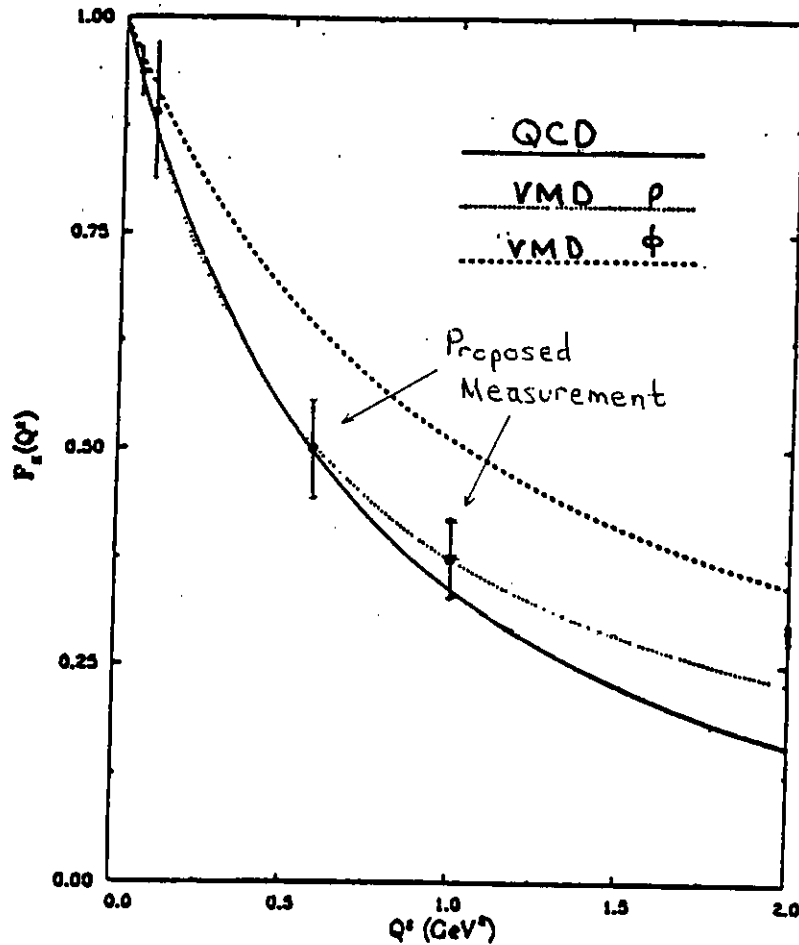


Figure 6. The kaon form factor plotted versus the momentum transfer squared. The present data extends only up to about $0.05 \text{ GeV}^2/c^2$. The three curves are explained in the text. This figure is taken from reference 23. Also shown are the two data points to be determined in this proposed experiment and the expected accuracy of the measurement.

Presented in Fig. 6 is the present knowledge of the kaon form factor. The data were obtained by scattering high energy kaons from atomic electrons. As can be seen, only a limited region in Q^2 can be accessed in this manner. The two dashed curves in the figure are from a parametrization of the form factor in the vector meson dominance model (VMD) of virtual photon scattering using rho and phi masses as indicated. This is explained in reference 23 which is where the figure was taken. The VMD model of this scattering assumes that the virtual photon converts into a vector meson before interacting with the target nucleon. The full curve in the figure is from a QCD inspired model. This experiment will test the Chew-Low extrapolation technique to determine $F_K(Q^2)$ at $Q^2 = 0.5$ and $1.0 \text{ GeV}^2/c^2$. This proposed experiment will gather data with sufficient precision to distinguish between the various models shown. This may indicate a QCD signature in nuclear physics. The proposed accuracy of the form factor determination is indicated in Fig. 6.

2.3 Out - of - Plane Kaon Electroproduction

Very little data have been published for σ_{LT} and σ_{TT} , the transverse-transverse and longitudinal-transverse cross sections, respectively, of equation (7)³⁸⁻⁴¹. The existing data (see Fig. 7) shows that both σ_{LT} and σ_{TT} are small compared to the σ_U and σ_L (roughly 10 %) for $K^+\Lambda$ production. This result implies that the cross sections for photons having their electric vectors parallel and perpendicular to the hadron production plane are roughly equal. For $K^+\Sigma^0$ production, measurements show that σ_{TT} can be negative, indicating that the cross section for photons with parallel electric vectors is smaller than that when the electric vector is perpendicular to the hadron production plane. At $Q^2 = 0.5 \text{ GeV}^2/c^2$ and $1.0 \text{ GeV}^2/c^2$, this experiment will separate σ_{LT} and σ_{TT} for fixed W . The t -dependence will then be measured.

3. EXPERIMENTAL DISCUSSION

3.1 Experimental Procedure

The proposed experiment to determine, separately, the four terms of Eqn. (7) from virtual photoproduction of kaons is ideally suited for Hall C using the High Momentum Spectrometer (HMS) to detect the scattered electron and the Short Orbit Spectrometer (SOS) to detect, in coincidence with the HMS, the electroproduced kaon before its decay in flight^{7,42}. An overview of Hall C in this mode is shown in Fig. 8.

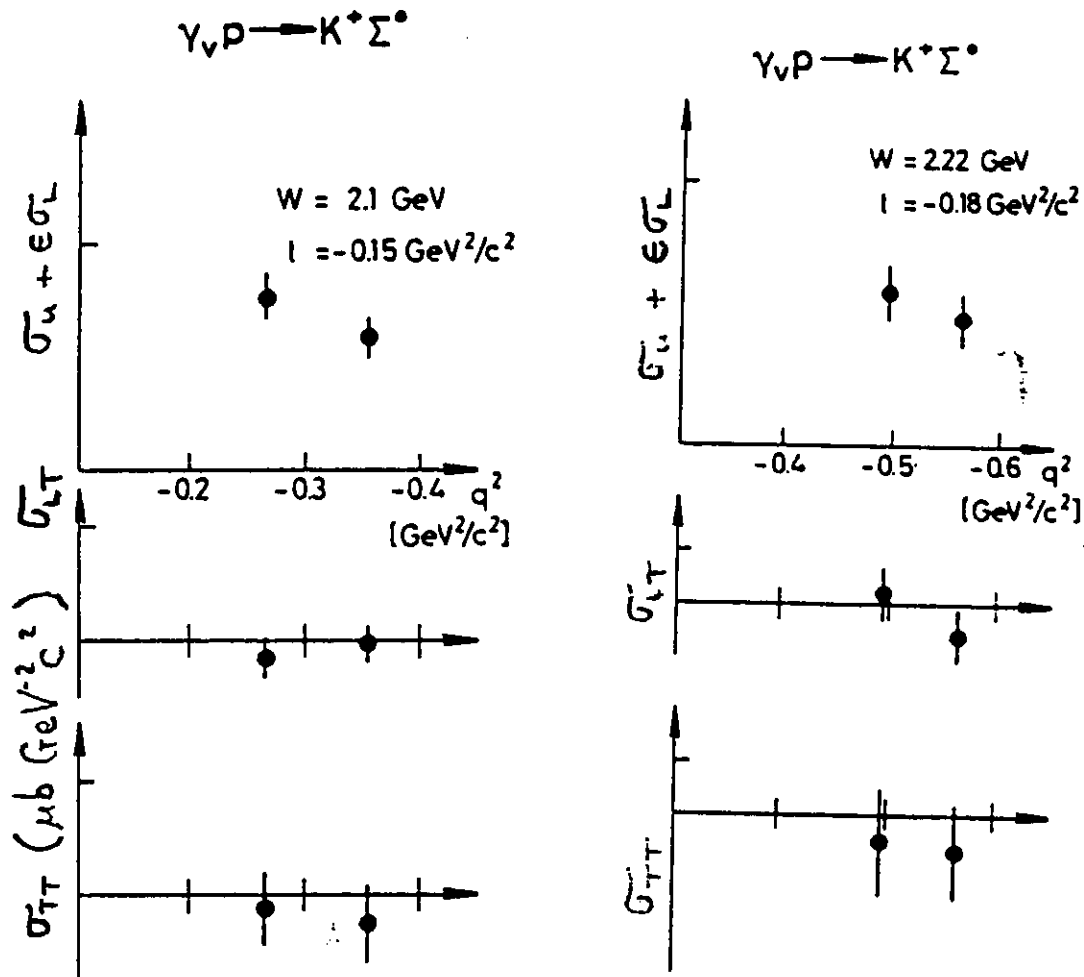


Figure 7. The available data on the out-of-plane cross sections extends only up to very low Q^2 as shown. The figure is from reference 38. The proposed experiment would extend the measurements up to Q^2 equal $1.0 \text{ GeV}^2/c^2$.

So far there has been only a crude attempt⁴³ to separate σ_U and σ_L . (See Fig. 9.) This longitudinal/transverse separation will be possible with the CEBAF beam and the spectrometers in Hall C. The longitudinal cross section, σ_L is related to the kaon form factor. Separation of the longitudinal contribution to the cross section, and therefore, the determination of the kaon form factor will depend upon the relative magnitudes of the first two terms in Eqn (21). (It would be more difficult to separate a very small contribution

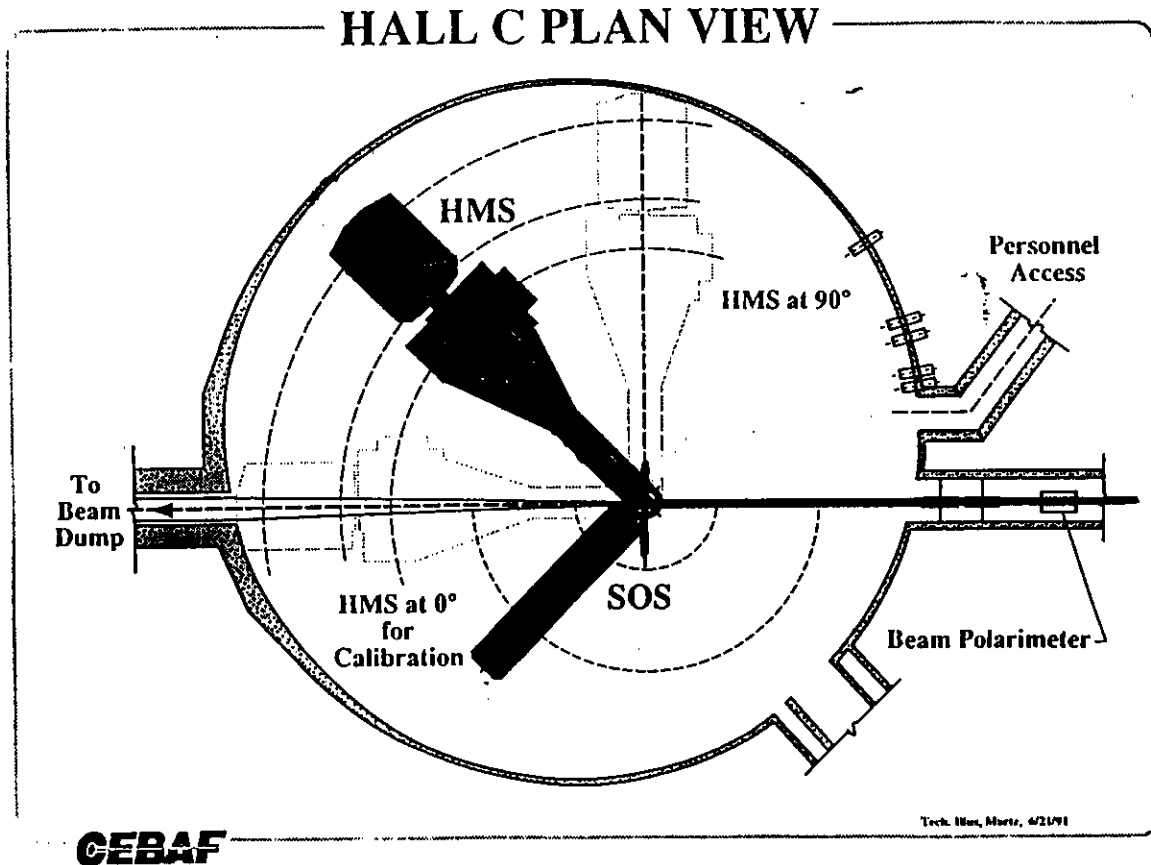


Figure 8. The Hall C setup using the HMS and SOS detectors. The scattered electrons will be detected in the HMS while the kaons will be detected in the SOS before their decay in flight.

from a relatively very large contribution).

Each of the terms has a small momentum-transfer-squared (Q^2) and angular (θ_{K^+}) dependence. These two separate contributions have not been measured accurately in the momentum transfer region of interest here. The large uncertainty in the data which exists presently doesn't allow too stringent a prediction to be made on their relative contributions; nevertheless, the trend of the data of reference 43 indicates that in the region of $Q^2 \leq$

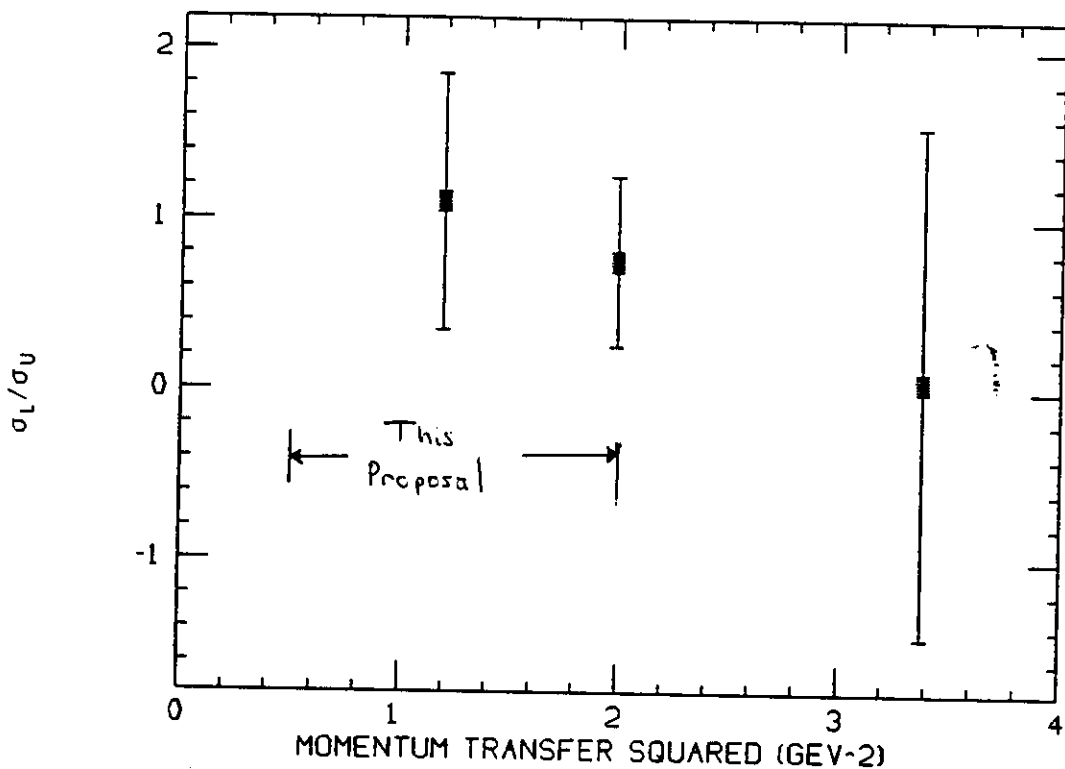


Figure 9. So far only a crude attempt has been made to separate the longitudinal and transverse cross sections as shown here. The data are from reference 43. Using the Hall C instruments, much more accurate data is possible as indicated.

4 GeV²/c², the unpolarized transverse contribution and that of the longitudinal polarized term are comparable. This proposed experiment would determine the cross section to \pm 5 % accuracy as shown.

A calculation has been made by Williams and Cotanch⁴⁴ of the cross sections given in Eqns. (17) and (18). The cross sections versus Q² and t are shown in Figs. 10 and 11 for (e,e'K⁺) with Λ and Σ final states.

Along the virtual photon direction, where the SOS spectrometer central axis will be positioned, the interference terms can be averaged to zero because of the finite acceptance of the SOS; it will be possible, therefore, to perform the required Rosenbluth separation

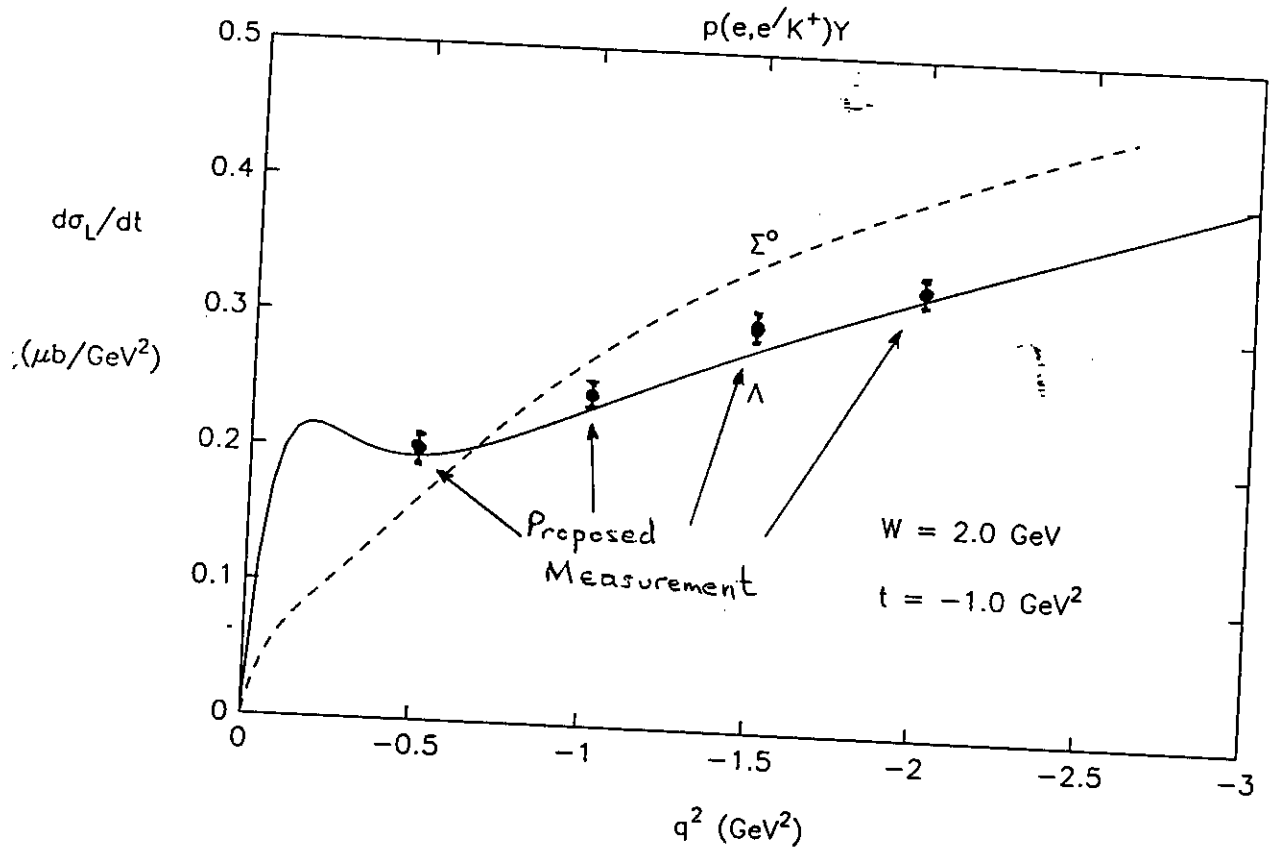


Figure 10. The longitudinal cross section in kaon electroproduction plotted versus q^2 . The calculation is from Williams and Cotanch (private communications). The range of q^2 accessed in this proposed experiment and the expected accuracy of the measurement is indicated for the $p(e, e'K^+)\Lambda$ reaction.

and single out the term in Eqn. (9) from longitudinally-polarized photons in a straightforward way. This separation is achieved by varying the virtual photon polarization, ϵ , and simultaneously averaging over all ϕ .

The Rosenbluth separation needed to separate the transverse and longitudinal cross sections will be implemented as follows: The SOS will be centered on the virtual photon direction. This means that the interference terms of Eqn. (9) (those terms proportional to $\cos\phi$ and $\cos 2\phi$) will average to zero because an average over the angle ϕ is effected by this arrangement. The remaining two terms, σ_U and $\epsilon\sigma_L$, are separated by varying ϵ , the virtual photon polarization parameter, between a high and low value. Additionally, to

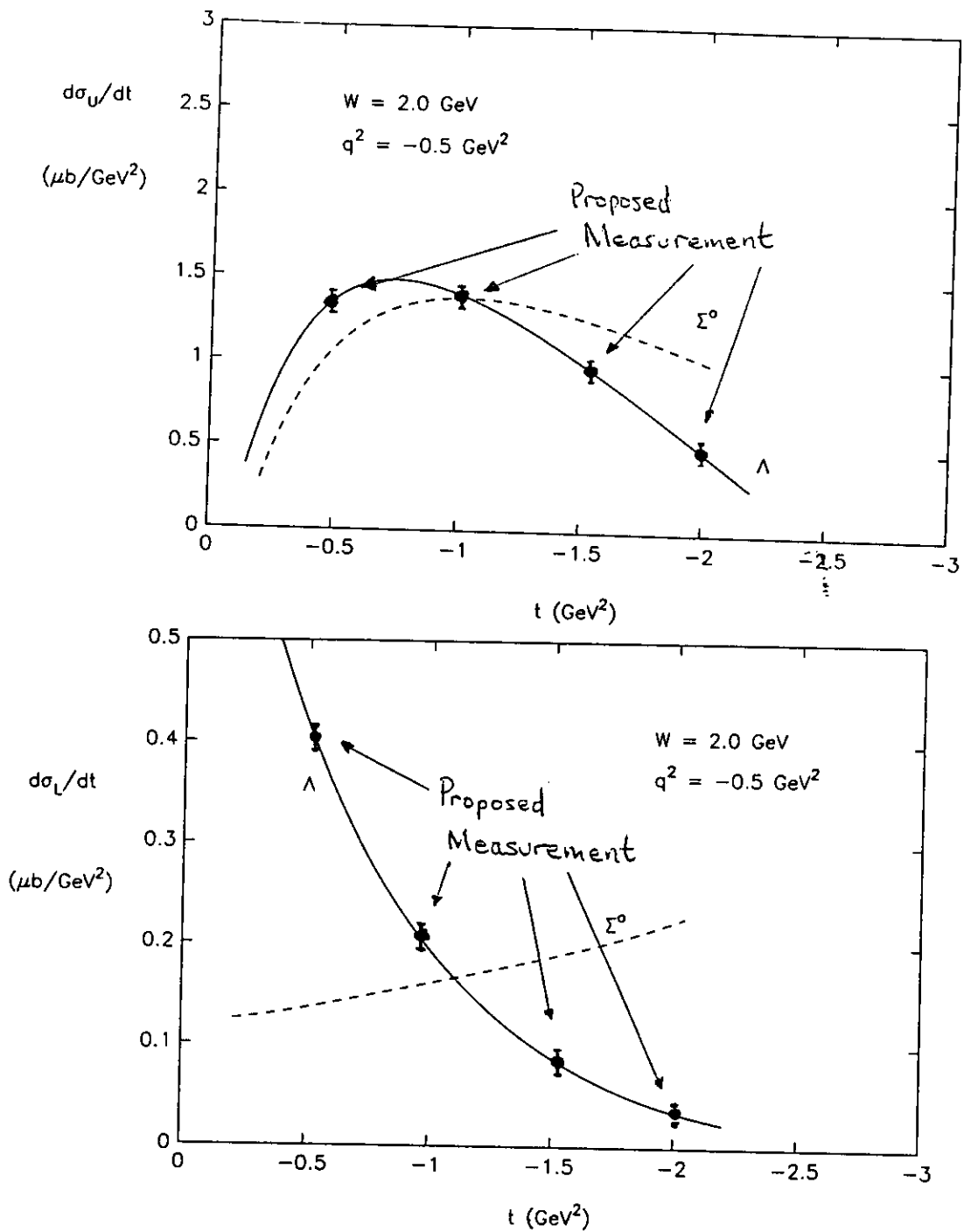


Figure 11. The longitudinal and transverse cross sections for $(e, e'K^+)$ plotted versus t . The calculation is from Williams and Cotanch (private communications). Also shown are the expected results of this proposed experiment.

extract the interference cross sections, the SOS will be positioned at each virtual photon angle, on opposite sides of the q direction so that $\cos\phi$ changes sign for identical data bins. Then σ_U , σ_L , and σ_{LT} are known, as is the experimental cross section, so that σ_{TT} can be extracted.

It is proposed to carry out this separation at Q^2 up to $2 \text{ GeV}^2/c^2$. The kinematic parameters for the separation are shown in Table I for representative kinematics. In

general, all values of ϵ between and including the ones shown in the Table are attainable. Once the first two terms of Eqn. (21) have been determined, the remaining interference terms can be determined at the same Q^2 and W by taking advantage of the ϕ dependence in these contributions. At each Q^2 , W point, the SOS will be positioned first on one side of the virtual photon direction, then on the other side, at an identical angle; that is, at fixed t . Then the four cross sections can be separated out versus t at each Q^2 and W point by varying the photon polarization parameter, ϵ .

The experiment can be used to measure the Bjorken x dependence of σ_U and σ_L as well. This measurement requires that the transverse and longitudinal cross sections defined above be separated (with the interference terms averaging to zero) while keeping Q^2 and W constant for each Q^2 setting. Table I shows the kinematic settings for this study while the kinematics points to be measured in Q^2 and ν (photon energy) is shown in Fig. 12.

TABLE I
Kinematic Parameters for x and Q^2 Dependences of σ_L and σ_U

Q^2	E_e	E'_e	θ_e	θ_γ	ν	W	x	ϵ
0.50	2.40	0.80	29.56	13.04	1.60	1.84	0.17	0.54
0.50	3.20	1.57	18.25	16.31	1.60	1.84	0.17	0.76
0.50	4.00	2.39	13.16	18.10	1.60	1.84	0.17	0.86
1.00	2.40	0.61	49.20	12.76	1.80	1.81	0.30	0.36
1.00	3.20	1.38	27.69	18.08	1.80	1.81	0.30	0.66
1.00	4.00	2.19	19.48	20.77	1.80	1.81	0.30	0.80
1.50	2.40	0.60	61.37	12.98	1.85	1.69	0.43	0.28
1.50	3.20	1.34	34.39	19.91	1.85	1.69	0.43	0.61
1.50	4.00	2.23	23.42	23.56	1.85	1.69	0.43	0.78
2.00	3.20	0.79	53.14	13.03	2.40	1.84	0.44	0.34
2.00	3.50	1.09	42.51	15.33	2.40	1.84	0.44	0.46
2.00	4.00	1.59	32.67	17.90	2.40	1.84	0.44	0.60

Energy in GeV; Momentum in GeV/c; Angles in Degrees

3.2 The t - dependence of σ_L and the Kaon Form Factor

In order to elucidate the proposed method for extracting the kaon electromagnetic form factor at high Q^2 using the Chew-Low extrapolation technique, it is instructive to begin with a discussion of previous experimental work in determining the pion form factor using this extrapolation procedure.

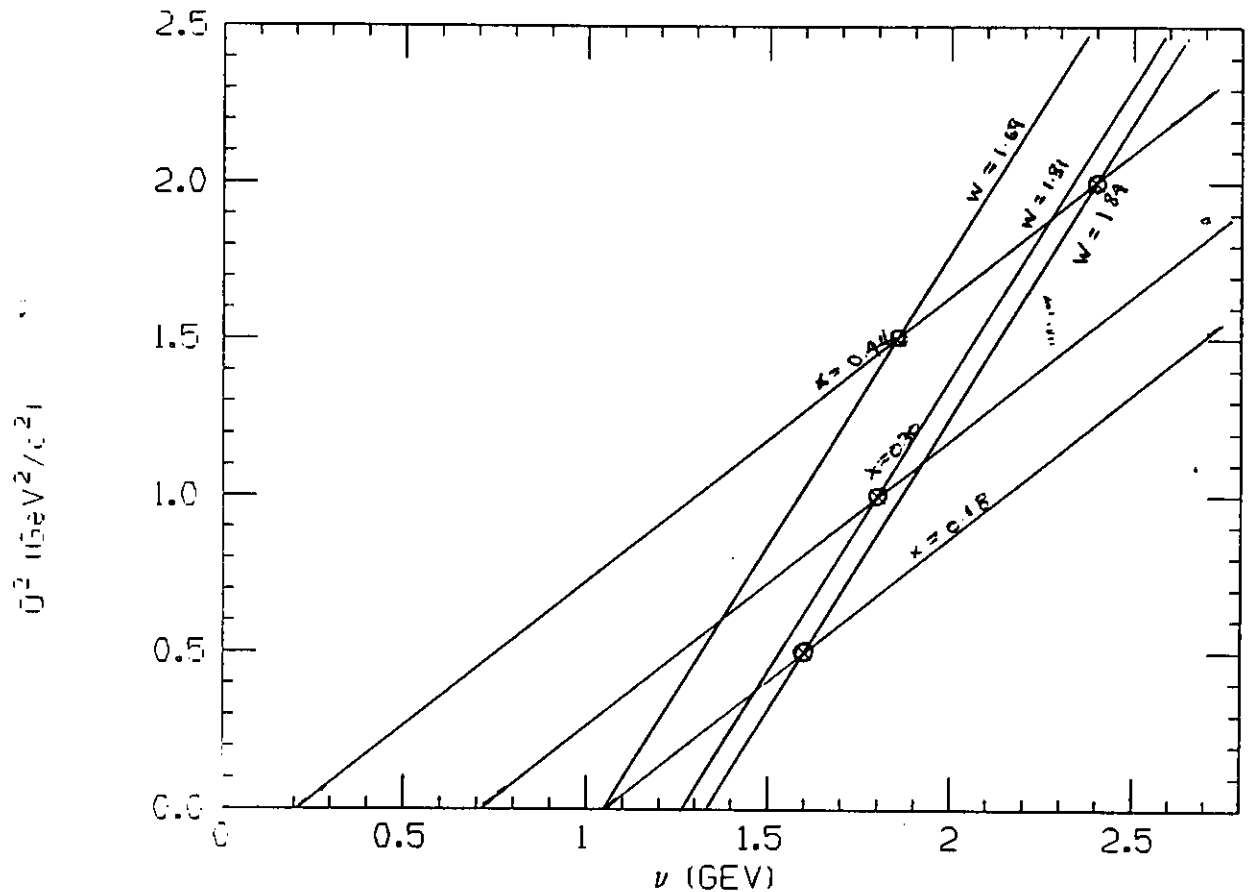


Figure 12. The kinematics used in the longitudinal and transverse cross section separations. The four points to be measured in this proposed experiment are circled.

As far back as 1959, it was suggested that the pion electromagnetic form factor, F_π , could be determined from π^+ electroproduction. As shown in Fig. 13, the cross-section-dependence on F_π comes in the one-pion-exchange pole diagram. This can be viewed as the elastic scattering of an electron from a virtual π^+ emitted by the target proton in the reaction

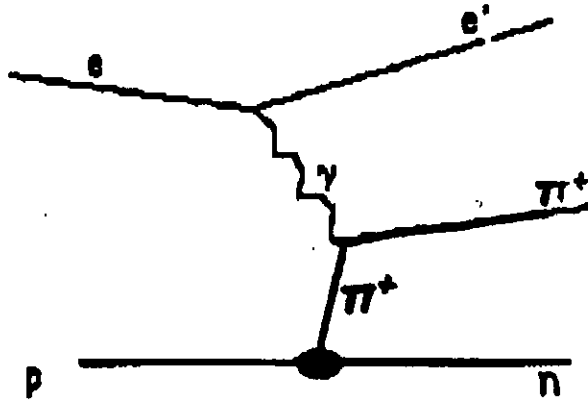


Figure 13. The coupling of a virtual photon to a virtual pion in pion electro-production

$$e + p \rightarrow e' + \pi^+ + n \quad (25)$$

or equivalently, in single virtual photon emission

$$\gamma_v + p \rightarrow \pi^+ + n. \quad (26)$$

In order to isolate the diagram from the others which would mask its effect and hence obscure F_π , it was proposed that an extrapolation of pion angular distribution data to the pion pole at $(p_\mu - p'_\mu)^2 = \mu^2$ be made. Then, because $\cos\theta_{\gamma_v\pi} = \frac{1}{\beta_\pi}$, this pole occurs at an unphysical angle; hence the extrapolation. This method requires the coincident detection of both scattered electron and electroproduced pion.

The pion yield is expressed in terms of the differential cross section $\frac{d^3\sigma}{dB'd\Omega_e d\Omega_\pi}$ where $d\Omega_e$ is the scattered-electron solid-angle in the laboratory, and $d\Omega_\pi$ is the pion solid-angle measured in the center-of-mass frame of the final pion and neutron. The resulting expression has the same form as that for kaon electroproduction

$$\frac{1}{\Gamma'_T} \frac{d^3\sigma}{dE' d\Omega_e d\Omega_{\pi^+}} = \frac{d\sigma}{d\Omega} |_{\pi^+} = \sigma_U + \epsilon\sigma_L + \epsilon\sigma_{TT} \cos 2\phi + \sqrt{\frac{\epsilon(\epsilon+1)}{2}} \sigma_{LT} \cos\phi \quad (27)$$

where

$$\Gamma'_T = \frac{\alpha}{2\pi^2} \frac{E'}{E} \frac{|\mathbf{k}|}{|k^2|} \frac{1}{1-\epsilon} \quad (28)$$

which is interpreted as the number of virtual photons per electron scattered into dE' and $d\Omega_e$. The factor $d\sigma/d\Omega_{\pi^+}$ is the center-of-mass differential cross section for pion photoproduction by virtual photons as discussed above in the context of kaon virtual photoproduction. The four terms are, just as discussed previously, those with cross sections from unpolarized transverse photons, longitudinal photons, the interference between transverse photons, and the interference between longitudinal and transverse photons, respectively.

In the coincidence pion electroproduction experiments performed to extract the pion electromagnetic form factor, the hadron spectrometer is centered on the virtual photon direction (or very nearly to it) so that the interference terms (on averaging in $\theta_{\gamma^* \pi^+}$) go to zero or are negligible. Then the transverse and longitudinal terms in the formula (σ_U and σ_L) are separated out by keeping the kinematic variables Q^2 , t , and W fixed. The results of this separation is illustrated in Fig. 14.

At each ϵ , an extrapolation in $t = -(\gamma^* - \pi^+)^2$ is performed by varying the angle $\theta_{\gamma^* \pi^+}$ between the virtual photon (fixed by the electron kinematics) and the detected pion in the hadron arm of the experiment. Thus σ_L can be separated at each value of t , allowing an extrapolation to the pion pole.

An example is shown in Fig. 15 for pion electroproduction. The position of the pion pole, $t = \mu^2$, is shown on the graph as a vertical dashed line. The intersection of this dashed line with the curves through the data should be proportional to F_π^2 , as shown in Fig. 16. It is expected that F_K^2 should be obtainable in a similar, albeit more difficult, way with perhaps greater uncertainty. Again, this separation has not been possible so far because σ_U and σ_L have not been separated.

From the formulas given in the appendix of Devenish et. al.²⁸, the residue of the kaon pole in the differential cross section can be calculated. Note that there is a $\sin\theta$ factor in the σ_{TT} term which must be removed in some way before the extrapolation is attempted because it has a square root branch point in t .

At the kaon pole, one has

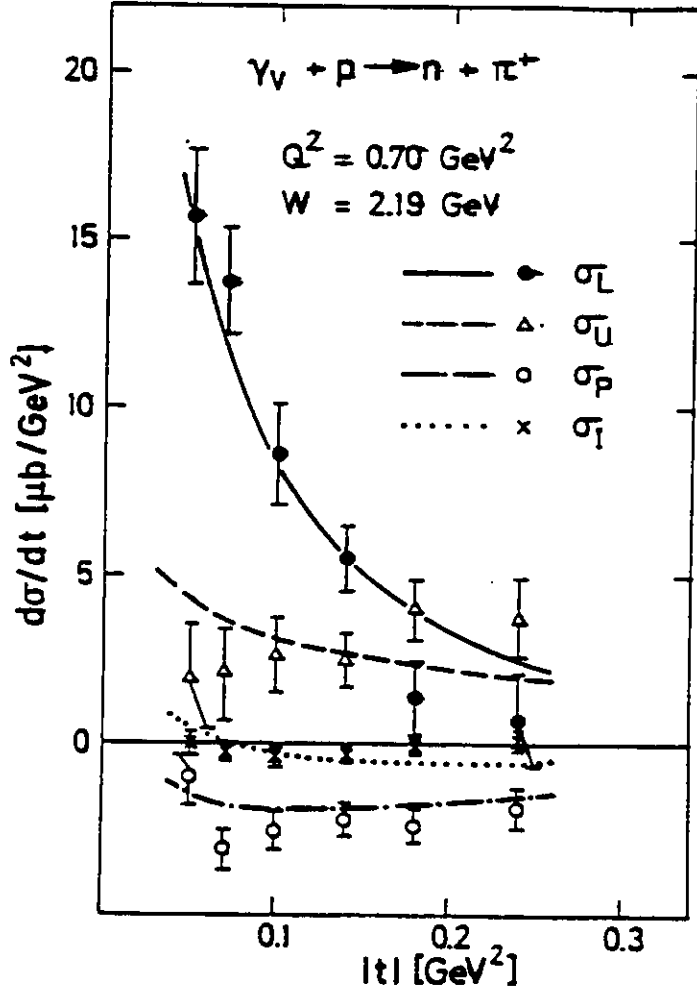


Figure 14. The separation of the four terms in the pion electroproduction cross section as shown in reference 21.

$$(t - \mu^2)^2 d\sigma|_{t=\mu^2} = N(\mu^2) F_K^2(Q^2) \quad (29)$$

where F_K is the kaon form factor, and

$$N(t) = (-t)8c(ge)^2(q^2 \sin^2 \theta) \left(\frac{1 + \epsilon \cos 2\phi}{2} \right) + \epsilon \frac{(|\mathbf{k}|E_{K^+} - k_o q \cos \theta)^2}{|\mathbf{k}|^2} \quad (30)$$

Here the constant c depends on the normalization of the data and is given, for example,

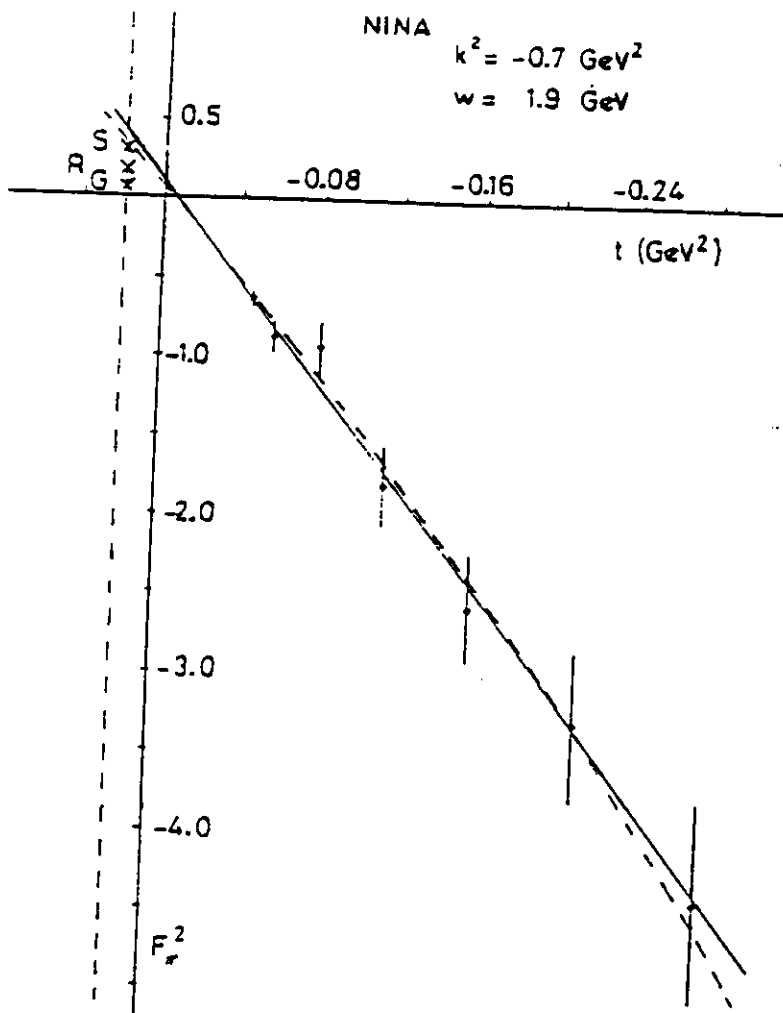


Figure 15. The extrapolation to the pion pole in the longitudinal cross section for pion electroproduction.

in the appendix of reference 28.

Each data point at fixed W and Q^2 will be multiplied by $(t - \mu^2)^2/N(\mu^2)$, and then the resulting points will be fit appropriately as shown in the next section.

The procedure assumes that the kaon pole, in this case, dominates the virtual photoproduction cross section for small t (close to t_{\min}). If the pole in the denominator is factored out of the experimental cross sections, the resulting data should lie on a smooth curve which can be extrapolated to the pole position in t . This procedure gives the residue

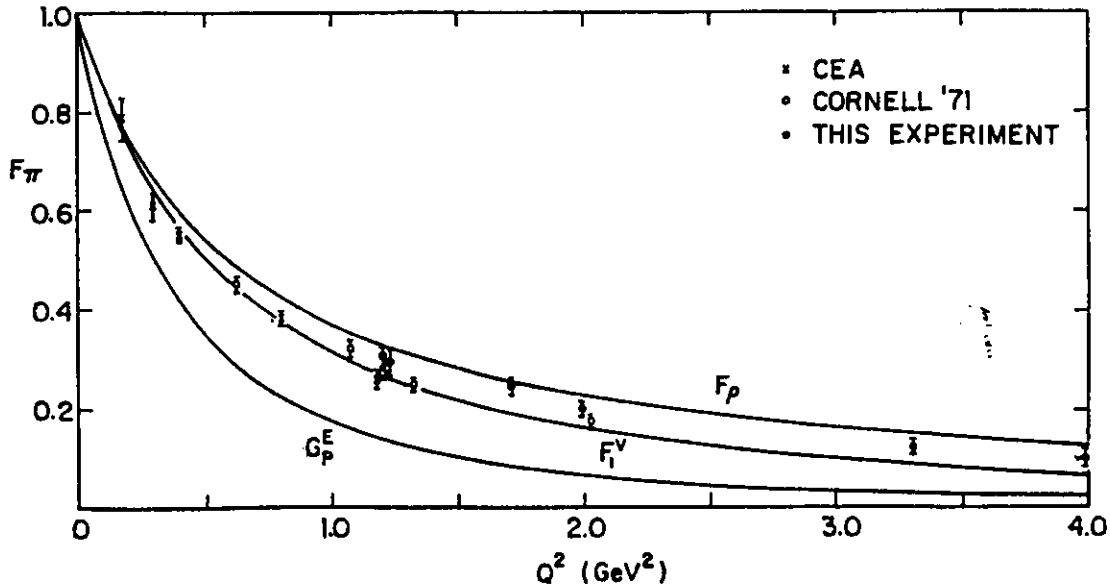


Figure 16. The pion electromagnetic form factor as determined by the Chew-Low extrapolation technique.

of the pole. If the coupling constants involved are known beforehand, then the kaon form factor can, in principle, be determined.

There has been previous work in measuring the t -dependence of the kaon electroproduction cross section for unseparated cross sections. These data are shown in Fig. 17. Also indicated on the figure is the range in t to be accessed in this present experiment.

Once the cross sections have been separated for each t point, the cross section will be multiplied by $(t - M_{K^+}^2)^2$ and N given above. The extrapolation in t for this quantity should give the kaon form factor at $t = M_{K^+}^2$. This is shown for the expected data points for the uncertainty expected in the measurement in Fig. 18. The uncertainties are shown in Tables II and III for the $Q^2 = 0.5$ and $1.0 \text{ GeV}^2/c^2$ points, respectively.

Future experiments might include a study of these separate contributions to kaon electroproduction on heavier nuclei⁴⁵⁻⁴⁶. The differences between these separate terms for

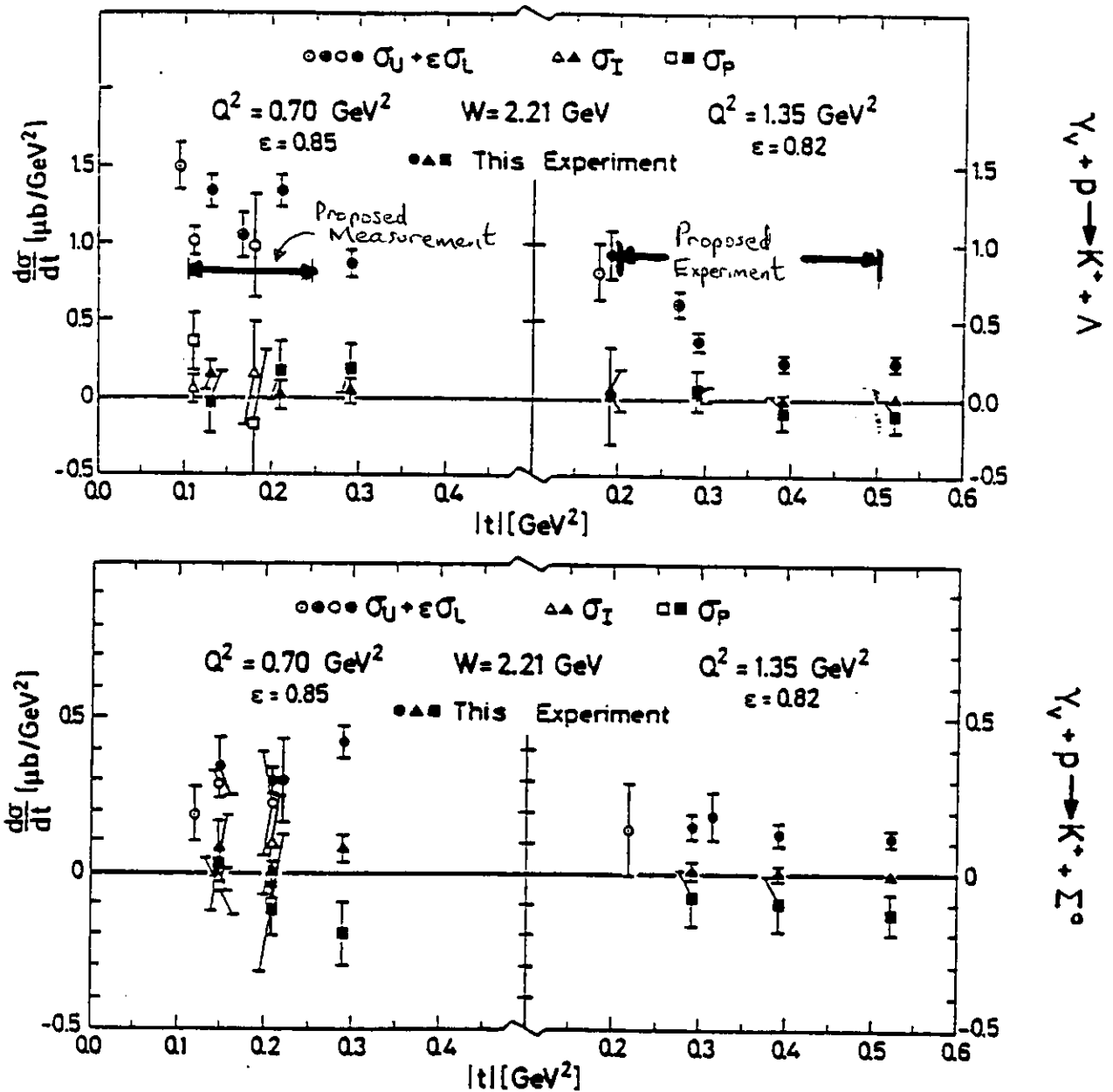


Figure 17. The cross section (unseparated) for kaon electroproduction when there is a Λ and a Σ particle in the final state versus t . The data are from reference 21. The range of t covered in this proposed experiment is indicated.

bare protons and those embedded in a nuclear medium may then be elucidated. Additionally, with a 6 GeV beam, it will be possible to access a broader range in ϵ , and at higher Q^2 .

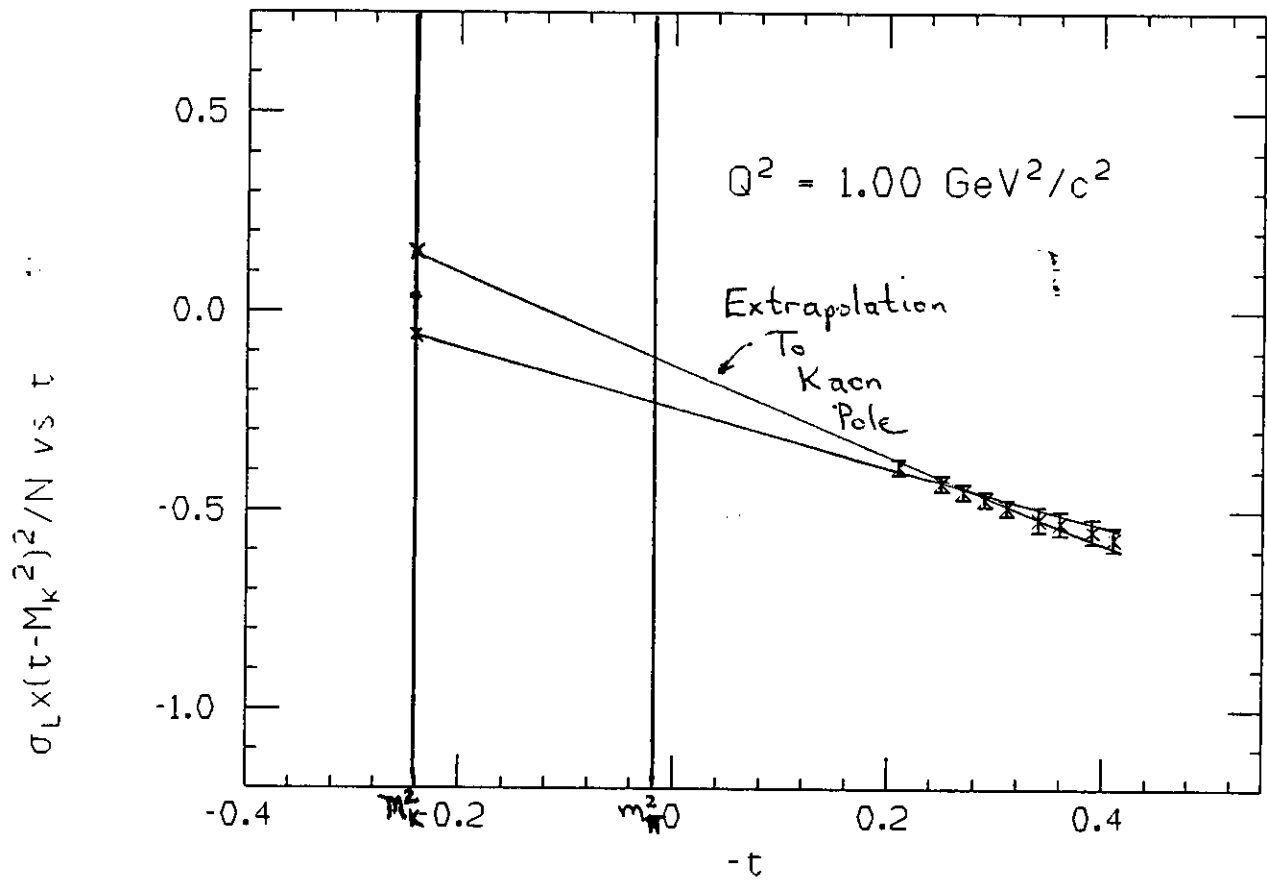


Figure 18. The expected t -extrapolation accuracy for the longitudinal cross section. The error bars include both the expected statistical and systematic uncertainties. The expected uncertainty in the kaon form factor determination is shown.

Thus it will be possible to determine these quantities, including the kaon electromagnetic form factor at higher Q^2 .

TABLE II

Kinematic Parameters for t Dependence of σ_L and σ_U at $Q^2 = 0.50 \text{ GeV}^2/c^2$

$$\begin{array}{llll}
 Q^2 = 0.65 & P_K = 1.40 & E_K = 1.48 & W = 1.90 \\
 P_{\gamma^*} = 1.97 & E_{\gamma^*} = 1.80 & x = 0.19 & t = 0.24
 \end{array}$$

E_e	E'_e	θ_e	θ_{γ^*}	Γ	ϵ
3.2	1.4	22.4	15.2	1.1	0.70
3.5	1.7	20.0	16.1	1.5	0.75
4.0	2.3	15.9	17.6	2.5	0.82

$$\begin{array}{llll}
 Q^2 = 0.50 & P_K = 1.43 & E_K = 1.51 & W = 1.94 \\
 P_{\gamma^*} = 1.93 & E_{\gamma^*} = 1.80 & x = 0.15 & t = 0.17
 \end{array}$$

E_e	E'_e	θ_e	θ_{γ^*}	Γ	ϵ
3.2	1.4	19.2	13.8	1.6	0.70
3.5	1.7	16.5	14.7	2.3	0.75
4.0	2.4	13.8	15.6	3.4	0.82

$$\begin{array}{llll}
 Q^2 = 0.35 & P_K = 1.46 & E_K = 1.54 & W = 1.98 \\
 P_{\gamma^*} = 1.90 & E_{\gamma^*} = 1.80 & x = 0.10 & t = 0.11
 \end{array}$$

E_e	E'_e	θ_e	θ_{γ^*}	Γ	ϵ
3.2	1.4	16.4	11.9	2.5	0.70
3.5	1.7	14.1	12.4	3.4	0.75
4.0	2.1	12.0	13.2	5.1	0.82

Energy in GeV; Momentum in GeV/c; Angles in Degrees

$$\begin{aligned}
 t - t_{\min} &= 4P_{\gamma^*}P_{K^+}\sin^2\theta/2 \\
 t_{\min} &= (E_{\gamma^*} - E_{K^+})^2 - (P_{\gamma^*} - P_{K^+})^2
 \end{aligned}$$

TABLE III

Kinematic Parameters for t Dependence of σ_L and σ_U at $Q^2 = 1.00 \text{ GeV}^2/c^2$

$$\begin{array}{llll}
 Q^2 = 1.25 & P_K = 1.54 & E_K = 1.62 & W = 1.87 \\
 P_{\gamma^*} = 2.34 & E_{\gamma^*} = 2.05 & x = 0.32 & t = 0.50
 \end{array}$$

E_e	E'_e	θ_e	θ_{γ^*}	Γ	ϵ
3.2	1.2	33.4	16.1	0.3	0.56
3.5	1.5	28.5	17.4	0.5	0.64
4.0	2.0	22.7	19.2	0.8	0.74

$$\begin{array}{llll}
 Q^2 = 1.00 & P_K = 1.62 & E_K = 1.69 & W \approx 1.93 \\
 P_{\gamma^*} = 2.28 & E_{\gamma^*} = 2.05 & x = 0.26 & t = 0.31
 \end{array}$$

E_e	E'_e	θ_e	θ_{γ^*}	Γ	ϵ
3.2	1.1	30.7	14.6	0.4	0.56
3.5	1.4	26.2	15.8	0.6	0.64
4.0	1.9	20.8	17.5	1.0	0.74

$$\begin{array}{llll}
 Q^2 = 0.75 & P_K = 1.67 & E_K = 1.74 & W = 1.99 \\
 P_{\gamma^*} = 2.22 & E_{\gamma^*} = 2.05 & x = 0.19 & t = 0.21
 \end{array}$$

E_e	E'_e	θ_e	θ_{γ^*}	Γ	ϵ
3.2	1.1	26.4	13.1	0.7	0.57
3.5	1.4	22.3	14.2	1.0	0.64
4.0	1.9	18.5	15.4	1.5	0.74

Energy in GeV; Momentum in GeV/c; Angles in Degrees

$$\begin{aligned}
 t - t_{\min} &= 4P_{\gamma^*}P_{K^+}\sin^2\theta/2 \\
 t_{\min} &= (E_{\gamma^*} - E_{K^+})^2 - (P_{\gamma^*} - P_{K^+})^2
 \end{aligned}$$

3.3 The HMS Detector and Background Estimates

The HMS is a QQQD focussing spectrometer. It will be used in the parallel-point tune mode. The quadrupole magnets serve to focus the scattered electrons, and therefore define the experimental solid angle, while the momentum determination is achieved by bending these same electrons in the dipole magnet. The largest contribution to the reconstructed electron momentum accuracy in the HMS resolution is $\frac{\Delta p}{p} \leq 10^{-3}$.

The detector stack for the HMS detector is shown in Fig. 19. The detector stack uses standard focal plane instrumentation and is detailed in the CEBAF Conceptual Design Report⁷. There will be drift chambers for charged particle tracking, a gas Cherenkov detector for particle identification, scintillator hodoscopes for fast timing, and Pb-glass shower counters for calorimetry. Each of these components has already been approved for construction and will be ready for use at the start of Hall C operation.

Charged particle trajectories will be measured using 2 multiwire drift chambers each having XYUVY'X' planes with the U and V stereo planes at 15° with respect to the X and X' planes. The X'(Y') planes are offset by 1/2 cell from the X(Y) planes. Thus there will be 12 multiwire planes before the scintillator hodoscopes or Cherenkov detector. The drift chambers will have cell sizes of 10 mm × 8 mm. Bench tests of the full sized HMS drift chambers have shown that spatial resolutions of better than 120 μ (σ) can be expected up to the highest rates that will be encountered in the experiments using the HMS. The acceptance is sufficient for this experiment (see Fig. 20).

The scintillator hodoscopes will be used for fast timing while the shower counters will be used for charged particle energy determination. The gas Cherenkov detector will be used for π-e and p-e discrimination. Additionally, there should be some separation of charged particles from the Pb:glass shower counters.

It is expected that pion-electron and proton-electron separations of 500/1 will be sufficient to reduce the backgrounds to acceptable levels⁴⁷.

It is expected that angular resolutions of less than 4 mrad are attainable with both the HMS and SOS detectors utilizing the drift chamber designs proposed. The effective solid angle of the HMS in the parallel-point tune versus momentum acceptance is shown in Fig. 21. The count rates given later use an average solid angle of 5 msr for a 6 cm long target. And, with momentum resolutions of $\leq 10^{-3}$ in each spectrometer, the uncertainties in angle and momentum measurements should be negligible when compared with other systematic and statistical uncertainties for a cross section measurement with $\pm 5\%$ accuracy.

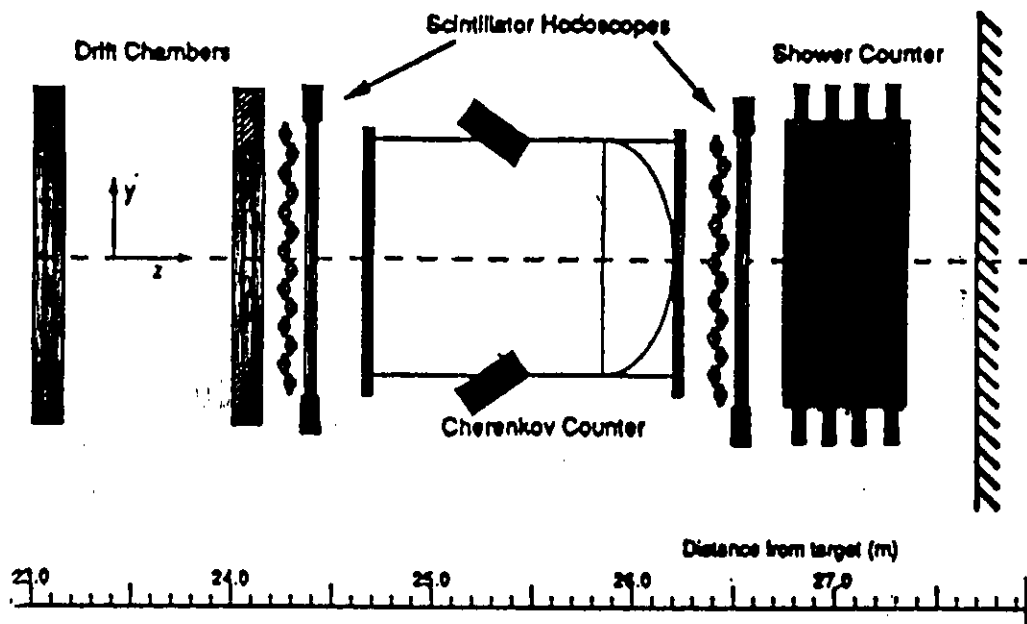


Figure 19. The detector stack proposed for the HMS spectrometer used in the coincidence experiment. This arrangement is the same as described in the CEBAF Conceptual Design Report.

TABLE IV
Time-of-Flight Differences for SOS Spectrometer*

Q^2 (GeV^2/c^2)	P_K (GeV)	$\Delta t(K - e)$	$\Delta t(K - \pi)$	$\Delta t(K - p)$
0.50	1.2	1.8	1.3	4.7
1.00	1.3	1.3	0.9	3.7
1.50	1.1	1.9	1.4	5.1
2.00	1.7	0.7	0.3	2.9

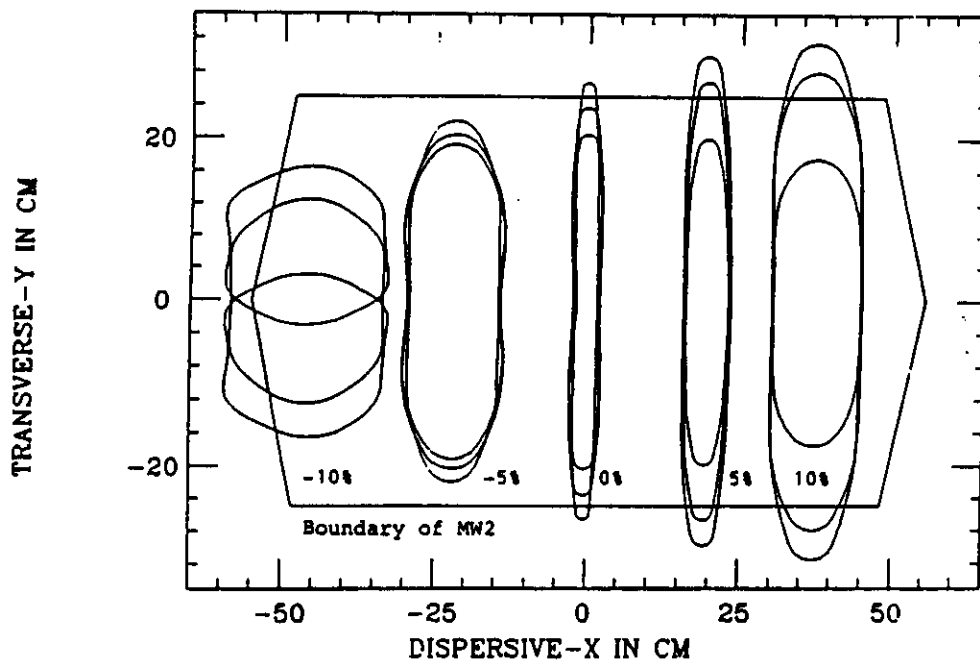


Figure 20. The acceptance of the HMS drift chambers for various particle trajectories through the spectrometer (parallel-point tune).

3.4 The SOS Detector and Background Estimates

The SOS is a QDD spectrometer with a very short flight path (compared to the HMS). This short flight path enhances the detection of the short-lived kaons before their in-flight decay. A sketch of the proposed detector stack is shown in Fig. 22.

The proposed SOS detector package consists of two sets of planar drift chambers, scintillator hodoscopes, a third drift chamber set followed by a second array of scintillators, an Aerogel Cherenkov counter, and finally a third set of XY scintillator planes. It is advantageous, in the SOS, to use the time-of-flight differences between protons, pions,

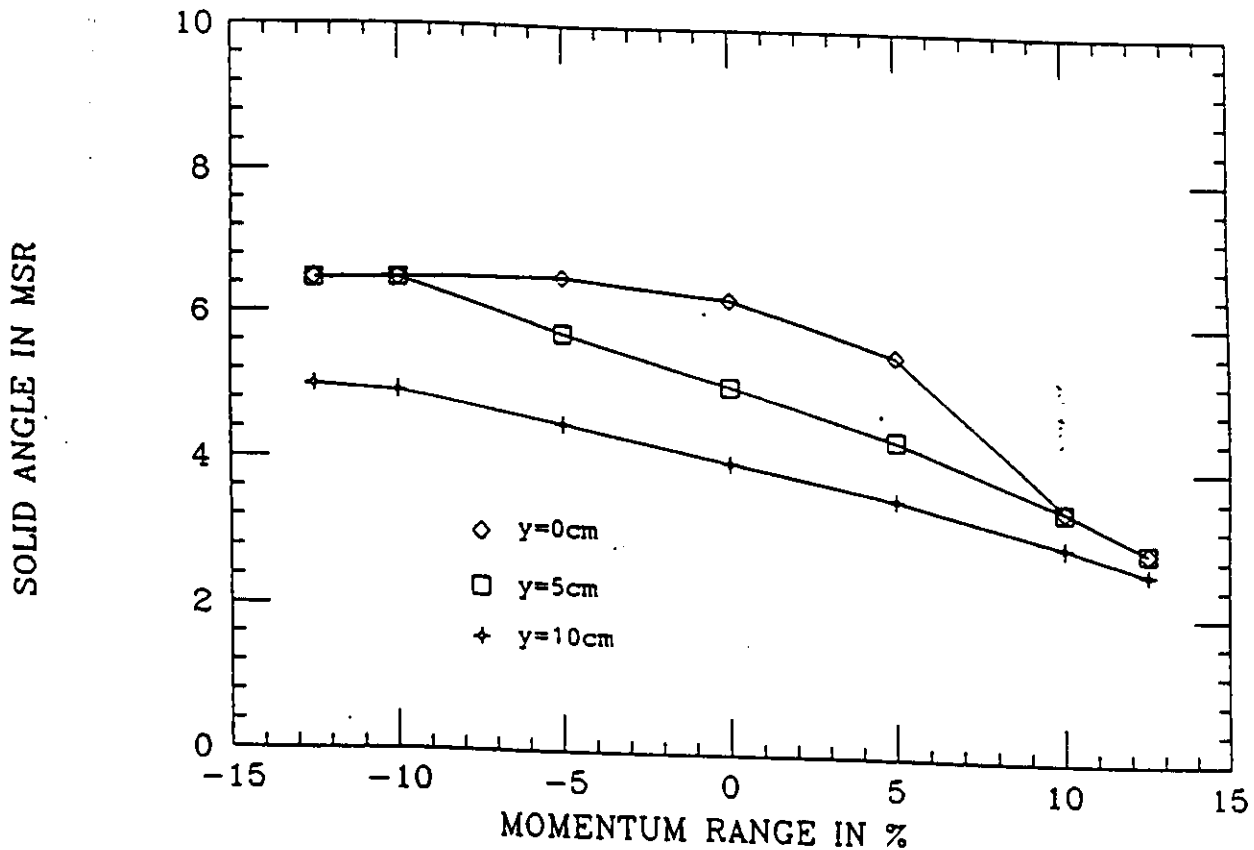


Figure 21. The HMS transmission response curve (parallel-point tune) versus momentum range for several target lengths.

kaons, and electrons to identify these charged particles (and therefore to separate them) at the lower spectrometer momentum settings. By maximizing the distance between the S1 and S3 scintillator arrays in the SOS detector hut, charged particle separation may be achieved. The time of flight differences for the various charged particles are listed in Table IV. Also see Fig. 23. The SOS acceptance is shown in Fig. 24.

The proton-kaon time difference is large enough at all momenta that the time difference may be resolved. For the higher momentum settings, judicious use of the Aerogel Cherenkov counter and some time-of-flight separation should adequately give a clean kaon signal. It is estimated that using this system, a pion rejection (the most insidious problem) of approximately 10^3 is achievable. This rejection ratio is expected to be adequate for this experiment⁴⁷.

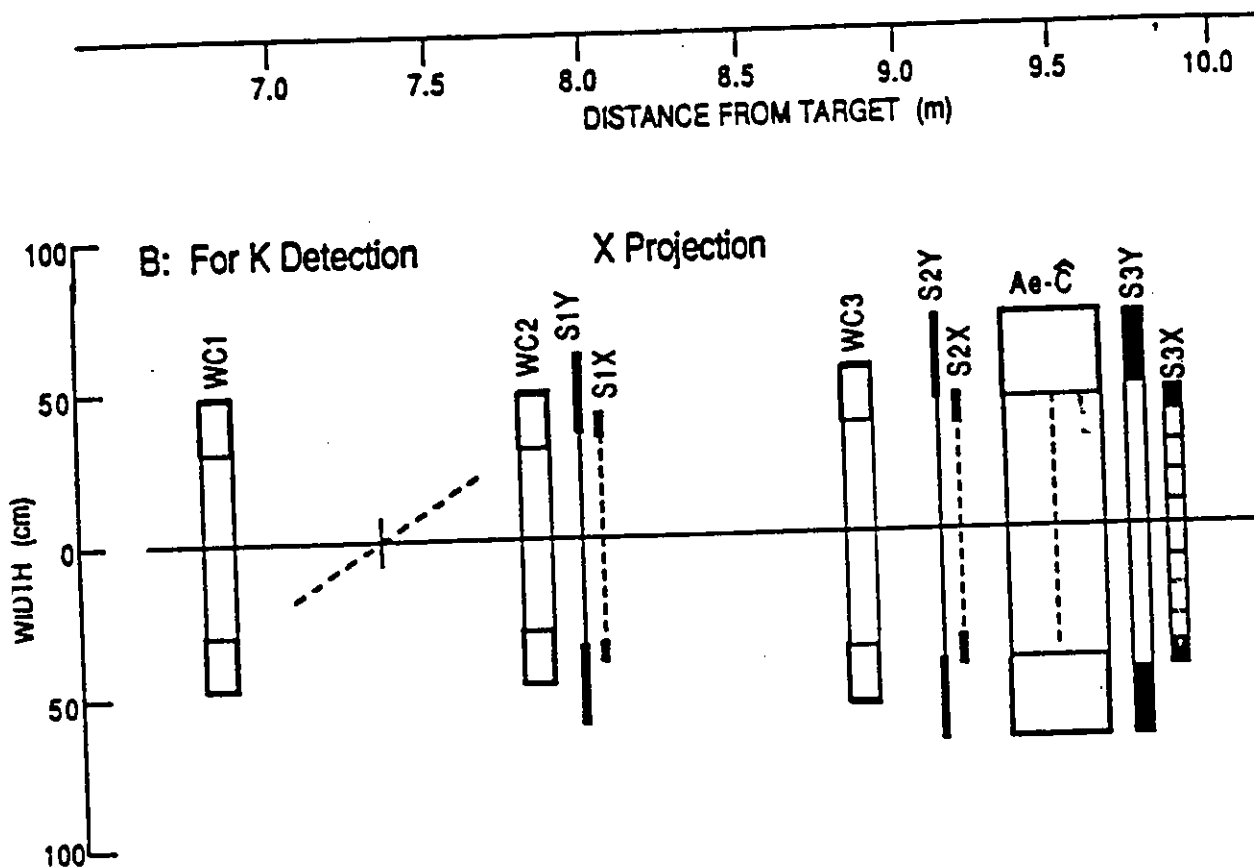


Figure 22. The detector stack proposed for the SOS spectrometer used in the coincidence experiment. This compliment of subsystems is the same as described in the CEBAF Conceptual Design Report.

The momentum of a charged particle will be determined by reconstructing its trajectory through the dipole (bending) magnet while the production angles are then obtained by tracing the trajectory through the quadrupole (focussing) magnets back to the target position. The maximum momentum acceptance is 20% (40%) while the average solid angle is 5 msr (3 msr) for the HMS (SOS) spectrometer using the parallel to point tune. This technique will be used for both arms of the experiment. In the SOS spectrometer, the acceptance is nearly flat over the entire momentum acceptance for a 6 cm long effective target as shown in Fig. 24.

3.5 The Hydrogen Target

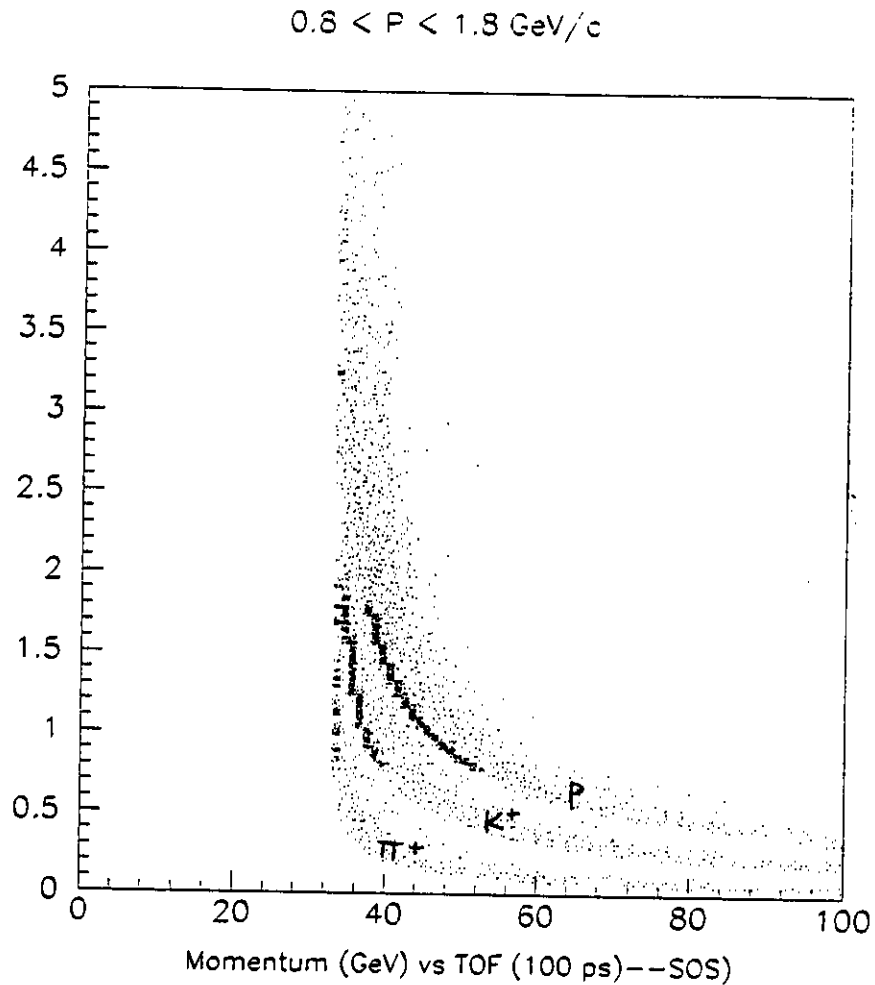


Figure 23. Geant simulation of the time of flight difference for one momentum setting in the SOS.

The hydrogen target planned for the experiment will be 15.0 cm in length and 6.4 cm in diameter. This target container, cylindrical in shape, will have 0.08 mm thick aluminum end-windows. The thickness of the sides is expected to be twice this value. The effective length as 'seen' by each spectrometer is calculated based upon Monte Carlo simulation.

The count rate results are shown in the tables which follow for each point to be measured. The uncertainty in the length of the target and target density is expected to be about 1 per cent. For the density, the calculated value based upon 21.5° K temperature and 32 psi pressure (operating parameters) is 0.070 g/cm³. For each point, a target empty and a target full run will be made.

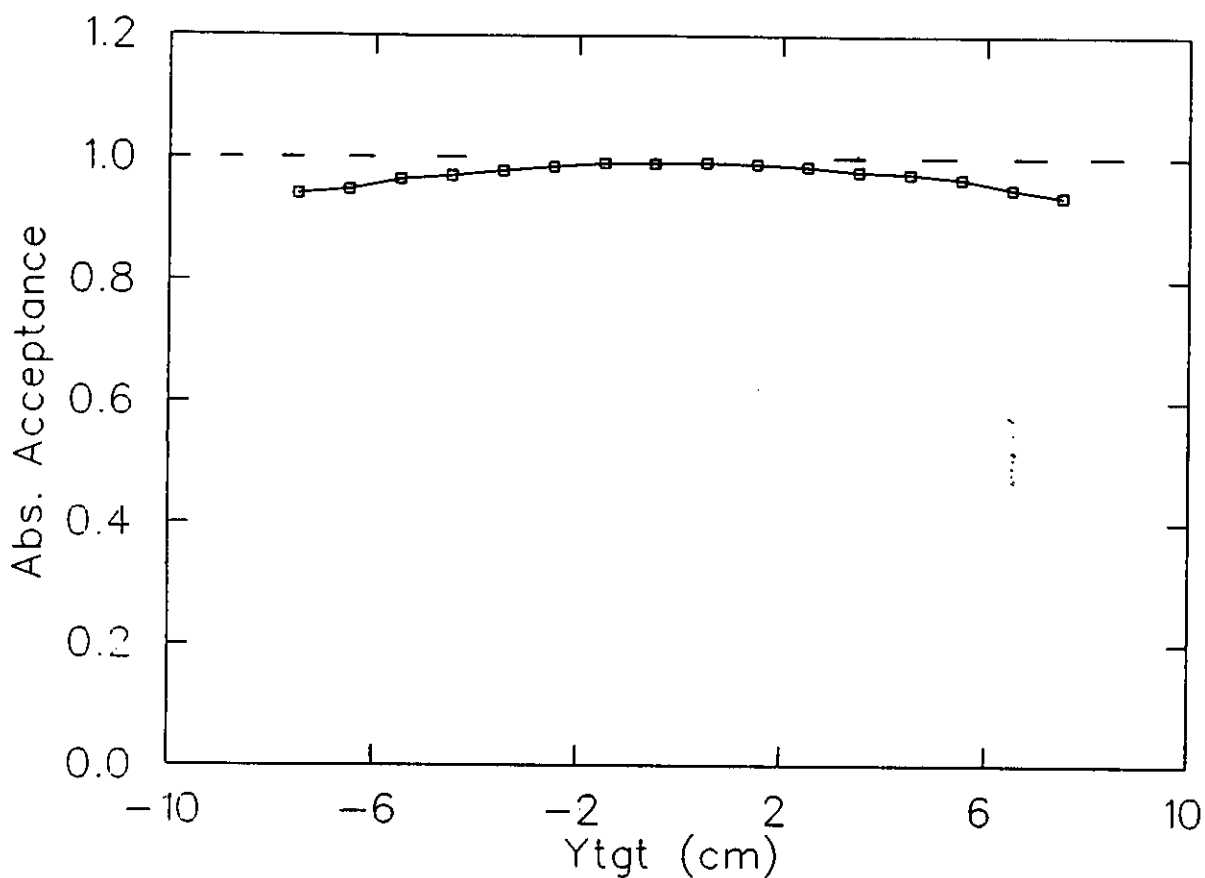


Figure 24. The SOS angular acceptance for a 40% momentum bite and 10 cm long target.

3.6 Electronics and Trigger

The experiment will use the CEBAF On Line Data Acquisition system (CODA) developed at CEBAF. The trigger in the HMS detector will consist of scintillator and Cherenkov hits to separate out electrons from pions and kaons (mainly) and antiprotons. Symbollically, the HMS trigger will be

$$S_1 \cdot S_2 \cdot C_e \cdot Sh \quad (31)$$

where S_1 (S_2) is the first (second) XY pair of scintillator hodoscopes, C_e is the gaseous Cherenkov detector which will fire on electrons and not pions or kaons, and Sh is the HMS shower counter. Time-of-flight separation will be adequate for $e - P$ and $e - K^-$ separation

at all momentum in the experiment for the HMS. The SOS will use a trigger to separate out kaons from pions, positrons, and protons mainly. Symbolically, the hadron arm trigger will be

$$S_1 \cdot S_2 \cdot \overline{C}_\pi \cdot Sh \quad (32)$$

where, again, S_1 (S_2) is the first (second) XY pair of scintillator hodoscopes, C_π is the aerogel Cherenkov detector (electronically in an anticoincidence mode), and Sh is the SOS shower counter. Time of flight separation is achievable at all but the few points at high kaon momenta as indicated in Table IV.

3.7 Expected Corrections

The cross sections defined in section 2 are each functions of Q^2 , W , and t . The separation this proposal aims to achieve requires that these variables are kept constant as ϵ is varied.

The uncertainty in Q^2 is given by the uncertainties in the incident and scattered electron energies and the scattering angles. When added in quadrature, the resulting uncertainty is $\pm 1\%$. From Fig. 3 the cross section in the range of interest here is seen to change by less than 5 percent, with $\frac{d\sigma}{d\Omega} = [Q^2 + 2.67]^{-2}$ for $(e,e'K^+)\Lambda$ and similarly, $\frac{d\sigma}{d\Omega} = [Q^2 + 0.785]^{-2}$ for $(e,e'K^+)\Sigma$.

There is a small W dependence in the region of interest in this experiment as shown in Fig. 25. For this measurement, for $\frac{\Delta W}{W} = \pm 5\%$, the cross section changes by less than $\pm 3\%$.

The uncertainty in t is given again by the uncertainties in electron energies and angles, but should be $\pm 1\%$. The t -dependence is expected to be rather smooth for the region of Q^2 and W of interest here as shown in Fig. 26 for $Q^2 = 1.0 \text{ GeV}^2/c^2$ and $W = 1.8 \text{ GeV}$. An uncertainty of less than $\pm 5\%$ is expected in the cross section.

Previous work in $p(e,e'K^+)$ experiments indicate that the detector stack will give uncertainties associated with each detector element as corrections are applied to the detectors. The corrections will be determined by Monte Carlo simulations and during the actual experiment. The expected uncertainties associated with the corrections are listed as follows.

Counter Dead Time	$\pm 2\%$
Wire Chamber Inefficiencies	$\pm 0.5\%$
Electron Shower Counter Inefficiencies	$\pm 1\%$

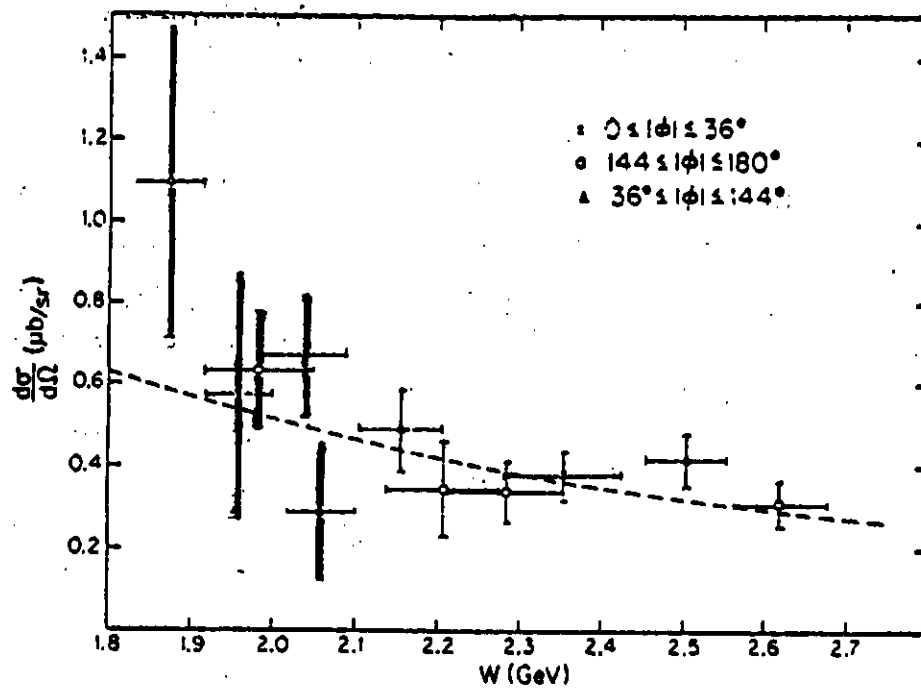


Figure 25. The W dependence of the center of mass cross section.

Kaon Absorption in the Target	+ 1 %
Kaon Arm Cherenkov-Counter Inefficiencies	+ 2 %
Kaon Decay	+ 3 %
Knock-on Events Firing Cherenkov	+ 1 %
Target Wall Events	+ 1 %
Randoms	+ 1 %
In Time Kaon Losses	+ 1 %
Radiative Corrections (Photon Radiations)	+ 3 %

Quadratic Sum + 5.7 %

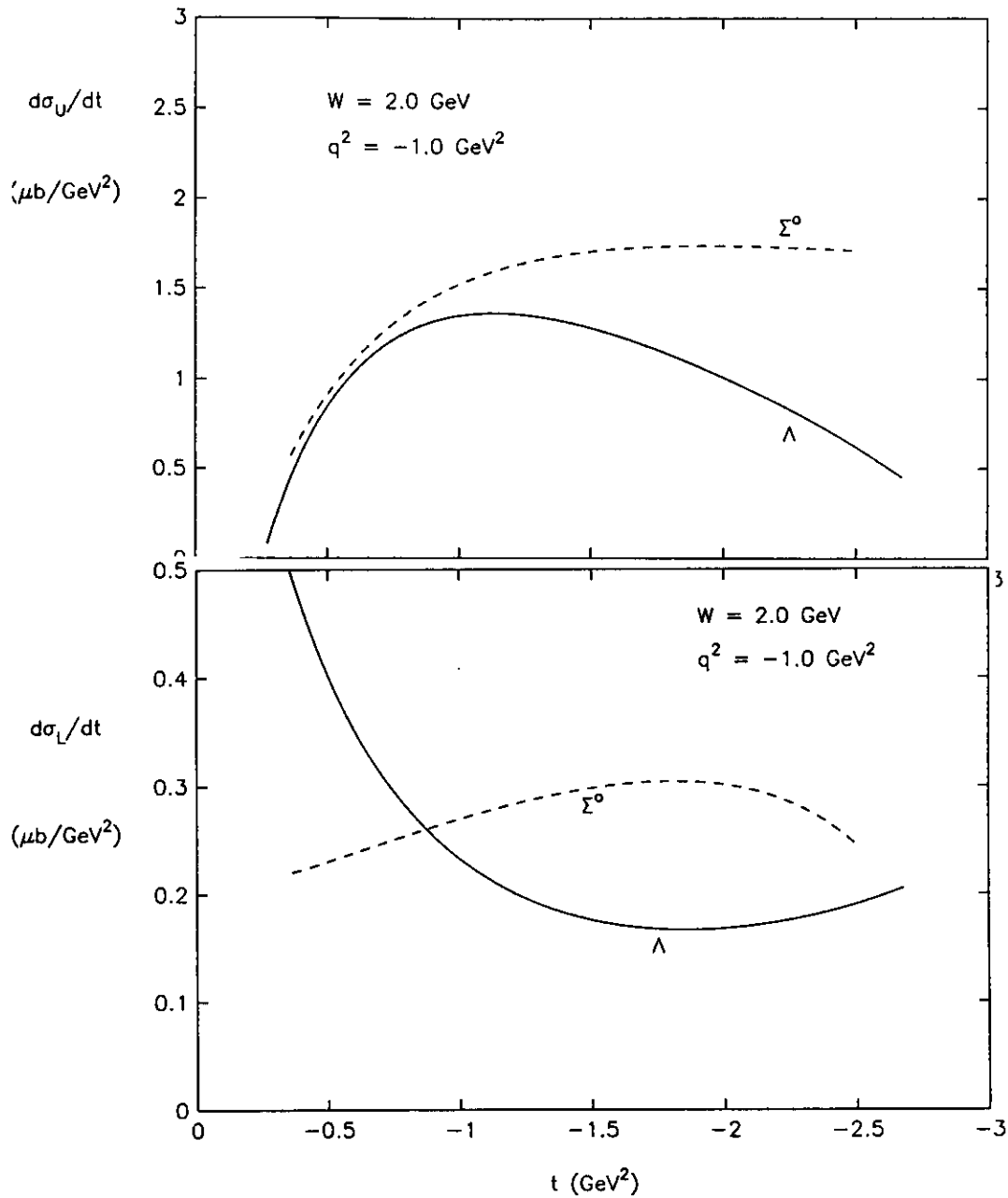


Figure 26. The calculated t -dependence of the longitudinal and transverse cross sections as calculated by Williams and Cotanch (private communications).

Note that this is approximately 6 % of the corrections which are expected to be about 30 - 40 %. The total systematic uncertainty due to the above corrections is expected to be about 2.5 %.

3.8 Rates And Beam Time Request

An estimate of the singles rates, R , in each of the spectrometers separately may be obtained from

$$R = n_i \cdot n_t \cdot t \cdot \frac{d\sigma}{d\Omega} \cdot \Delta\Omega \cdot (1 - P_{\text{decay}}) \quad (33)$$

where n_i is the number of incident particles per second on a target of thickness t and target density n_t . $d\sigma/d\Omega$ is the scattering cross section and $\Delta\Omega$ is the spectrometer solid angle. The count rate is corrected for kaon survival probability (see Fig. 27).

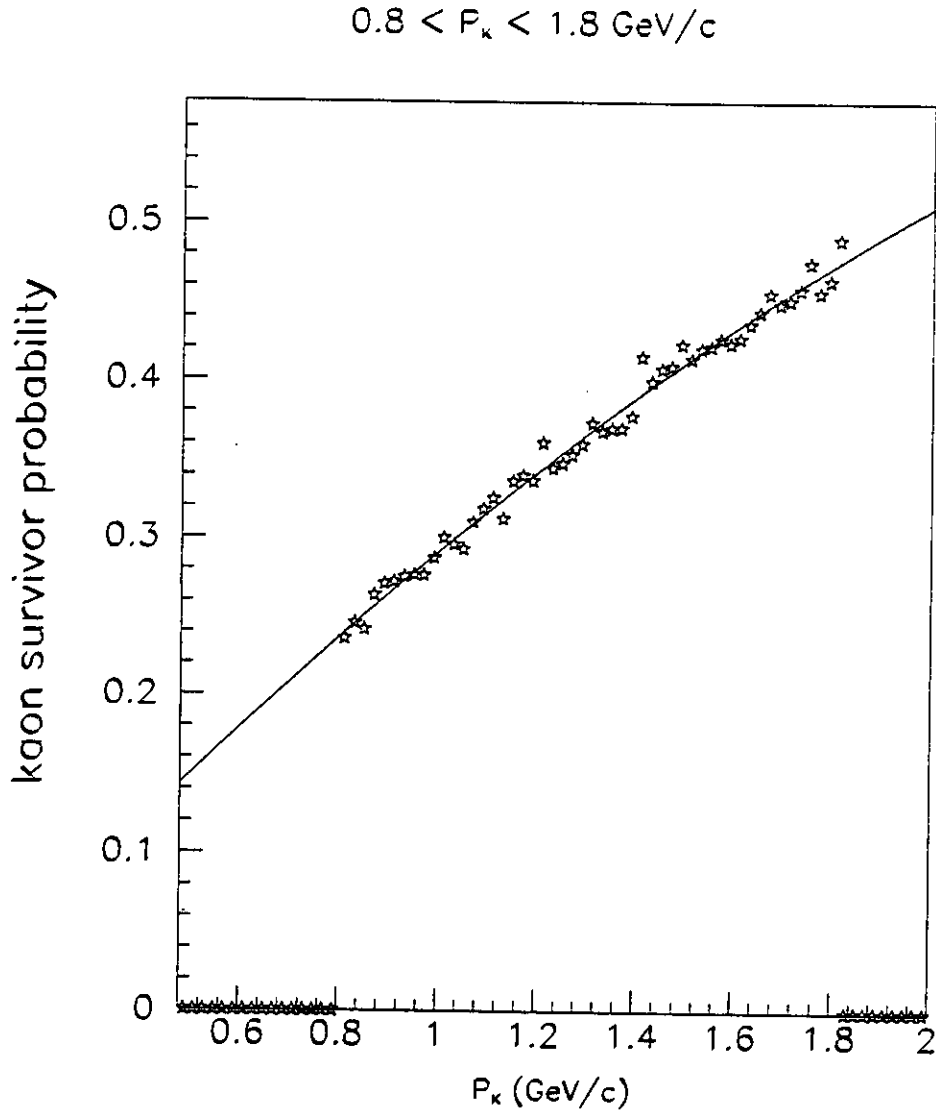


Figure 27. Geant simulation of the kaon survival probability in the SOS detector for one momentum setting.

In the electron arm, the Mott cross section formula for $d\sigma/d\Omega$ is used in calculating the

rates. The cross sections were compared with those from the Lightbody and O'Connell code⁴⁸ and found to agree to within a few percent. The rates are shown in Table V. Preliminary results from the prototype drift chamber studies using the drift cells described in reference 49 indicate that these rates will cause no difficulty for the charged particle tracking. For the hadron arm, cross sections are estimated using the results from references 21 and 43. The center of mass cross sections, multiplied by the photon flux factor (Γ) yields the experimental cross section as shown in equations (17) and (18). The triple and quadruple differential cross sections are then integrated over the kinematic acceptance of the SOS spectrometer, yielding the differential cross section for kaon electroproduction $\frac{d\sigma}{d\Omega}$. Then equation (33) is used to calculate the singles rates in the SOS as shown in Table VI.

TABLE V
HMS Singles Counting Rates*

Q^2 (GeV ² /c ²)	ϵ	θ_e	I (μ A)	Rate (kHz)
0.50	0.54	29.6	30	30
0.50	0.76	18.2	30	120
0.50	0.86	13.2	30	240
1.00	0.36	49.2	50	20
1.00	0.66	27.7	30	42
1.00	0.80	19.5	30	240
1.50	0.28	61.4	30	30
1.50	0.61	34.4	30	12
1.50	0.78	23.4	30	140
2.00	0.34	53.1	50	5
2.00	0.46	42.5	50	15
2.00	0.60	32.7	50	15

* Liquid hydrogen target; angles in degrees.

The coincidence rate, R_{coinc} , for the HMS and SOS used in this experiment is estimated from the formula²³:

$$R_{\text{coinc}} = \frac{i}{e} \cdot \frac{\rho t N_o}{A} \cdot \epsilon_D \cdot \frac{d^3\sigma}{dE_e d\Omega_e d\Omega_k} \cdot \Delta E_e \Delta \Omega_e \Delta \Omega_k (1 - P_{\text{decay}}) \quad (34)$$

Here $\Delta\Omega$ is the solid angle of the spectrometer, ϵ_D is the detection efficiency, i is the beam current, N_o is Avogadro's number, e is the electron charge, t is the target thickness of mass number A and density ρ . For the HMS spectrometer, $\Delta E/E$ will be about 20%. For a

hydrogen target, a 100 nb cross section [24-25] for kaon electroproduction, and a 10 μA of beam, a coincidence rate of about 0.5 counts per second is expected, for example.

TABLE VI
SOS Singles Counting Rates*

Q^2 (GeV^2/c^2)	ϵ	θ_{γ^*}	I (μA)	Rate (Hz)
0.50	0.54	13.0	30	120
0.50	0.76	16.3	30	480
0.50	0.86	18.1	30	960
1.00	0.36	12.8	50	80
1.00	0.66	18.1	30	170
1.00	0.80	20.8	30	960
1.50	0.28	13.0	30	12
1.50	0.61	19.9	30	48
1.50	0.78	23.6	30	560
2.00	0.34	13.0	50	20
2.00	0.46	15.3	50	60
2.00	0.60	17.9	50	60

* Liquid hydrogen target. $\theta_{\gamma^*K^+} = 0^\circ$; angles in degrees.

An estimate of the number of accidental to true coincidences A/T is obtained from

$$\frac{A}{T} = \frac{\tau R_e R_k}{f R_{\text{coinc}}} \quad (35)$$

where the duty factor f is 1 for the CEBAF facility and the resolving time, τ , is taken to be 2.5 ns offline and 10 ns online. Although A/T could be reduced somewhat by lowering the beam current (at the expense of counting rates), this ratio should allow a 5% measurement without difficulty.

TABLE VII
Coincidence Rates*

Q^2	ϵ	R_{Coinc} (Hz)	*A/T	+A/T	Time (Days)
0.50	0.50	0.10	0.4	0.10	1.0
0.50	0.70	1.00	1.0	0.20	0.5
0.50	0.80	2.00	1.0	0.20	0.5
1.00	0.50	0.10	0.2	0.04	1.0
1.00	0.70	0.1	0.7	0.10	0.5
1.00	0.90	2.00	1.0	0.20	0.5
1.50	0.40	0.06	0.1	0.02	1.0
1.50	0.60	0.06	0.1	0.02	1.0
1.50	0.90	1.00	1.0	0.20	0.5
2.00	0.40	0.02	0.1	0.02	1.0
2.00	0.60	0.06	0.1	0.02	1.0
2.00	0.90	0.06	0.1	0.02	1.0

* 10 ns resolving time online.

+ 2 ns resolving time offline.

A measurement at the momentum transfer proposed here with the statistics required will require approximately 14.5 days of running. This is summarized in Table VIII.

TABLE VIII
Beam Time Request

	Time (Days)
Data Acquisition	9.5
Setup and Checkout	1.0
Angle Changes	0.2
Background Studies	2.0
Contingency (15%)	1.8
TOTAL	14.5

3.9 The Collaboration

The collaboration includes institutions and personnel that have made substantial contributions to building hardware and readying software for the experiment. This expertise

allows this to be a first generation experiment. Additionally, not listed here are several graduate students who will use this experiment as part of their dissertation research. The Hampton University group has built the HMS multiwire drift chambers for Hall C. This group has 6 graduate students, 1 postdoc and 2 (presently) faculty members involved in experimental work, and 2 faculty, 1 postdoc, and several students providing theoretical support. Other institutions provide similar levels of effort as part of this collaboration.

REFERENCES

1. J. D. Walecka, Argonne National Lab. Report ANL-83-50 (1983).
2. S. Nozawa and T. S. Lee, Nucl. Phys. A513, 511 (1990).
3. W. E. Kleppinger and J. D. Walecka, Ann. Phys. 146, 349 (1983).
4. T. De Forest, Jr., Ann. Phys. 45, 365 (1967).
5. G. Gourdin, IL Nuovo Cim. 221, 1094 (1961).
6. D. R. Yennie et. al., Rev. Mod. Phys. 29, 144 (1957).
7. CEBAF Conceptual Design Report, (1990).
8. See for example R. K. Bhaduri, *Models of the Nucleon*, Addison-Wesley Publ. Co., Menlo Park, CA (1988).
9. C. B. Dover and D. J. Millener, Phys. Rep. 184, 1 (1989).
10. C. Benhold, Phys. Rev. C39, 1944 (1989).
11. M. Moinester et. al., Phys. Rev. C46, 1 (1992).
12. S. Cotanch, Proc. Int. Conf. Med. and High Energy Nucl. Phys., 666 (1989).
13. W. Koepf et. al., Phys. Lett. B 238, 11 (1992).
14. R. Schumacher, Inv. Talk at "Part. Prod. Near Thresh", Ind. Univ (1990).
15. R. E. Chrien and C. B. Dover, Ann. Rev. Nucl. Part. Sci. 39, 113 (1989).
16. O. K. Baker, CEBAF Experimental Proposal 91-022, (1991).
17. E. Amaldi et. al., *Pion Electroproduction*, Springer-Verlag Publishing Co., N. Y. (197
18. C. J. Bebek et. al. Phys. Rev. D15, 594 (1977).
19. O. Nachtman, Nucl. Phys. B74, 422 (1974).
20. J. Cleymans and F. Close, Nucl. Phys. B85, 429 (1975).
21. P. Brauel et. al., Z. Phy. C, Part. Fields, 3, 101 (1979).
22. C.J. Bebek et. al., Phys. Rev., Lett. 32, 21 (1974).
23. C. Ji and R. Cotanch, Phys. Rev. D 41, 2319 (1990).
24. S. R. Amendolia et. al., Phys. Lett. B 178, 435 (1986).
25. F. Felicetti and Y. Srivastava, Phys. Lett. 107B, 227 (1981).
26. M. Lutz and W. Weise, Nucl. Phys. A518, 156 (1990).
27. C. W. Akerlof et. al., Phys. Rev. D16, 147 (1966).
28. R. C. E. Devenish and D. H. Lyth, Phys. Rev. D5, 47 (1972).
29. F. Gutbrod and G. Kramer, Nucl. Phys. B49, 461 (1972).
30. C. N. Brown et. al., Phys. Rev. D 8, 91 (1973).
31. R. H. Dalitz and D. R. Yennie, Phys. Rev. 105, 1598 (1957).
32. W. Frazer, Phys. Rev. 115, 1763 (1959).
33. C. W. Akerlof et. al., Phys. Rev. 163, 1482 (1967).
34. L. Hand, Phys. Rev. 129, 1834 (1963).
35. F. A. Berends and G. B. West, Phys. Rev. 188, 2538 (1969).
36. F. A. Berends, Phys. Rev D1, 2590 (1970).

37. C. J. Bebek et. al., Phys. Rev. D 17, 1693 (1978).
38. T. Azemoon et. al., Nucl. Phys. B95, 77 (1975).
39. A. Bartl and W. Majerotto, Nucl. Phys. B90, 285 (1975).
40. N. Levy et. al., Nucl. Phys. B55, 513 (1973).
41. J. W. V. Orden, CEBAF Summer Workshop, (1992).
42. C. Yan et. al., HMS Users Manual, CEBAF (1991).
43. C. J. Bebek et. al., Phys. Rev. D 15, 3082 (1977).
44. R. Williams and S. Cotanch, private communications, (1993).
45. S. R. Cotanch and S. S. Hsiao, Nucl. Phys. A 450, 4192 (1986).
46. T. W. Donnelly, CEBAF Summer Workshop (1984).
47. B. Zeidman, pri. comm. (1991).
48. See also J. W. Lightbody, Jr. and J. S. O'Connell, Comp. In Phys. 2, 5 (1988).
49. O. K. Baker et. al., IEEE Proceed (1991).